Title: Control of eukaryotic phosphate homeostasis by inositol polyphosphate sensor domains.

Authors: Rebekka Wild[1,†], Ruta Gerasimaite[2,†], Ji-Yul Jung[3,†], Vincent Truffault[4], Igor Pavlovic[5], Andrea Schmidt[2], Adolfo Saiardi[6], Henning Jacob Jessen[5,7], Yves Poirier[3,*], Michael Hothorn[1,*], Andreas Mayer[2,*]

Affiliations:

[1]Structural Plant Biology Laboratory, Department of Botany and Plant Biology, University of Geneva, Switzerland.

[2]Department of Biochemistry, University of Lausanne, Switzerland.

[3]Department of Plant Molecular Biology, University of Lausanne, Switzerland.

[4]Department of Biochemistry, Max Planck Institute for Developmental Biology, Tübingen, Germany.

[5]Department of Chemistry and Pharmacy, University of Zürich, Switzerland.

[6]Medical Research Council Laboratory for Molecular Cell Biology, University College London, U.K..

[7]Institute of Organic Chemistry, Albert-Ludwigs-University Freiburg, Germany.

*Correspondence to: yves.poirier@unil.ch (Y.P.), michael.hothorn@unige.ch (M.H.), andreas.mayer@unil.ch (A.M.)

†These authors contributed equally to this study.

Abstract: Phosphorus is a macronutrient taken up by cells as inorganic phosphate (P_i). How cells sense cellular P_i levels is poorly characterized. Here we report that SPX domains, which are found in eukaryotic phosphate transporters, signaling proteins and inorganic polyphosphate polymerases, provide a basic binding surface for inositol polyphosphate signaling molecules (InsPs), whose concentrations change in response to P_i availability. Substitutions of critical binding surface residues impair InsP binding *in vitro*, inorganic polyphosphate synthesis in yeast and P_i transport in Arabidopsis. In plants, InsPs trigger the association of SPX proteins with transcription factors to regulate P_i starvation responses. We propose that InsPs communicate cytosolic P_i levels to SPX domains and enable them to interact with a multitude of proteins to regulate P_i uptake, transport and storage in fungi, plants and animals. (130 words)

One Sentence Summary: A conserved protein domain allows cells to sense internal phosphate and regulate its uptake via binding inositol polyphosphates. (128 characters)

Main Text: P_i uptake, transport, storage and signaling systems in eukaryotes (*1*, *2*) are supported by proteins containing SPX domains of unknown function (*3*). These small domains (135 – 380 residues) are located at the N-termini of P_i transporters (*4–7*), the inorganic polyphosphate (polyP) polymerase **V**acuolar **T**ransporter **C**haperone (VTC) (*8*) and P_i signaling proteins (*9*, *10*), or occur as independent, single-domain proteins (*11*) (Fig. S1). Mutations in the SPX domain in plant and human P_i exporters impair their transport capacity and affect P_i signaling (*12*). The P_i transporters Pho87 and Pho90 interact via their SPX domains with the yeast Spl2 protein and this interaction down-regulates P_i uptake (*4, 13*) (Fig. S1). In plants, SPX domains bind **PH**OSPHATE STARVATION **R**ESPONSE (PHR) transcription factors, which mediate P_i starvation-induced gene expression under P_i limiting conditions (*11, 14*). Formation of a SPX domain – PHR complex prevents the transcription factor from binding its target promoters, thus reducing the expression of starvation-induced genes under P_i-sufficient growth conditions (*15, 16*). P_i itself may promote the association of SPX proteins with PHRs and thus SPX domains may sense cellular P_i levels (*15, 16*).

To investigate if SPX domains are eukaryotic sensors for P_i, we mapped their domain boundaries and expressed and purified fungal, plant and human SPX domains (Fig. S2). We determined three independent crystal structures of SPX^{ScVtc4} (residues 1-178) from the yeast VTC complex (*8*) at 2.1 - 3.0 Å resolution (Table S1). Structures of the SPX domain of the *C. thermophilum* glycerophosphodiesterase (residues 1-184) and of the human phosphate transporter XPR1 (**X**enotropic and **P**olytropic retrovirus **R**eceptor 1; residues 1-207) were solved at 1.95 Å and 2.43 Å resolution, respectively. These structures highlight key features of the SPX domain: Its core consists of two long (~80 Å) helices α3 and α4 connected by linkers of variable length (Fig. 1A,B). The core helices and two smaller C-terminal helices α5 and α6 contribute to the formation of a 3-helix bundle (Fig. 1A,B). Helix α6 adopts various orientations in our different structures (Figs. 1B, S3). The N-terminus of the domain folds into a helical hairpin formed by α1 and α2, but in several 'apo' structures helix α1 appears disordered (Fig. 1A,B). SPX domains share no significant structural homology with proteins of known function (*17*).

We located a conserved basic surface cluster at the N-terminus of the SPX helical bundle (Fig. 1C). Several invariant Lys residues and $Tyr22^{HsXPR1}$ from helices α2 and α4 represent SPX sequence fingerprints and contribute to the formation of the surface cluster (Figs. 1C,D, S2) (*3*). A sulfate ion is bound to a pocket in the surface cluster of SPX^{HsXPR1} (Fig. 1D). SO_4^{2-}, which in crystal structures is often bound in place of P_i, is coordinated by the back bone amides of Lys2, Phe3 and Ala4 from helix

α1, by Tyr22 and Lys26 from α2 and by Lys162 from α4 (**P**hosphate **B**inding **C**luster, PBC) in SPX^{HsXPR1} (Fig. 1D). Residues in contact with SO_4^{2-} are invariant among SPX domains from different eukaryotes (Fig. S2) and thus the sulfate ion could mark the previously suggested P_i binding site (*15, 16*).

NMR titrations of wild-type SPX^{ScVtc2} and SPX^{HsXPR1} revealed a K_d for P_i of ~ 5 and 20 mM, respectively (Figs. 1E, S4). Mutation of PBC residues in SPX^{ScVtc2} reduces P_i binding, as does deletion of the N-terminal α1 helix (ΔN14) or reductive methylation of surface lysines (Fig. 1E). The reduced binding affinity of the ΔN14 mutant, the observed structural changes in our SPX domain crystal structures and the number of peak shifts in the NMR titration experiments indicate that SPX domains undergo conformational changes upon ligand binding, possibly involving the α1 helix (Figs. 1A-E, S3, S4). In contrast to earlier reports (*15, 16*), we find that SPX^{ScVtc2} cannot discriminate between P_i and sulfate (Figs. 1E, S4). Also, the SPX basic surface cluster contains many more conserved lysine residues than required for P_i coordination (**L**ysine **S**urface **C**luster, KSC; $Lys^{ScVtc2}127$, $Lys^{ScVtc2}130$, $Lys^{ScVtc2}134$) and mutation of all three KSC lysines to Ala has no effect on P_i binding (Figs. 1D,E, S4). Larger ligands, such as pyrophosphate (PP_i) interact more tightly with SPX^{ScVtc2} (Figs. 1E, S4). Thus, SPX domains harbor a large, positively charged surface able to interact with a phosphate-containing ligand, but show little specificity and selectivity for P_i itself.

In order to define other potential ligands for eukaryotic SPX domains, we analyzed polyP synthesis in isolated yeast vacuoles, which is catalyzed by the SPX-containing VTC complex and regulated by P_i levels *in vivo*. Deletion of the $InsP_6$ kinase Kcs1, which produces inositol pyrophosphate (PP-InsP) signaling molecules, eliminates VTC-generated polyP stores (Fig. S5) (*18–20*). We synthesized 5-$InsP_7$, a Kcs1 reaction product, and found that it stimulated VTC-catalyzed polyP synthesis at concentrations above 100 nM (Figs. 2A, S5). In contrast, P_i and SO_4^{2-} activated VTC only at millimolar concentrations (Fig. 2A). SPX^{ScVtc2} and other SPX domains bind 5-$InsP_7$ and $InsP_6$ with ~50 – 500 nanomolar affinity and with 1:1 binding stoichiometry in different *in vitro* assays (Figs. 2B, S4, S6, Table S2). SPX^{ScVtc2} discriminates between 5-$InsP_7$/$InsP_6$ and $InsP_5$, $InsP_4$ or $InsP_3$ and consequently these molecules cannot stimulate VTC-catalyzed polyP synthesis (Figs. S6, S7, Table S2).

Isolated SPX domains recognize 5-$InsP_7$ and $InsP_6$ with similar binding affinities ~~and $InsP_6$ stimulates VTC activity above 100 μM~~. We thus used $InsP_6$ in our subsequent crystallization experiments as a commercially available substitute for 5-$InsP_7$, of which we could only synthesize low milligram quantities. Complex structures of SPX^{CtGde1} and SPX^{CtVtc4} reveal that $InsP_6$ interacts with the basic

surface cluster via variable hydrogen-bond interactions (Figs. 2C-F, S8, Table S1). This results in a high structural plasticity of the binding site, as seen in pleckstrin homology domains (*21*). The C2-attached axial phosphate group of $InsP_6$ is anchored in the PBC pocket occupied by SO_4^{2-} in the SPX^{HsXPR1} structure (Figs. 1D, 2C-F, S8). PBC and KSC residues together form the SPX InsP binding site (Fig. 2C-F). Additional hydrogen bonds with $InsP_6$ are established by the N-terminal amino group and by main-chain atoms from residues 1-4 in helix α1 (Fig. 2F). Binding of InsP ligands may thus stabilize the SPX α-helical hairpin motif.

Substitution of conserved surface cluster residues reduced $InsP_6$ and 5-$InsP_7$ binding to SPX^{ScVtc2} *in vitro* (Figs. 3A,B, S9, Table S3). Corresponding mutations in SPX^{ScVtc3} and SPX^{ScVtc4} in yeast cells abolished stimulation of polyP synthesis by 5-$InsP_7$, while mutation of $Lys126^{ScVtc3}$/$Lys129^{ScVtc4}$ to Ala constitutively activated polyP production (Fig. 3C). Thus, VTC polyP synthesis is controlled by its SPX domains and InsPs, rationalizing previous genetic findings (*18, 22*).

The Arabidopsis PHOSPHATE 1 (PHO1) protein, an orthologue of the human XPR1 P_i exporter, controls P_i transport from the root to the shoot and P_i-starvation responses (*5, 23*). We substituted InsP-binding residues in the SPX^{AtPHO1} basic surface cluster and complemented the *pho1* knock-out phenotype (*5*) with these mutant AtPHO1 constructs. K136 → Ala control plants resembled plants transformed with a wild-type AtPHO1 construct, while the PBC, KSC and ΔN15 mutants showed reduced growth (Figs. 3D, S10). PBC and KSC plants had very similar phenotypes, suggesting that the entire surface cluster and not only the PBC residues are required for normal SPX domain function of AtPHO1 *in vivo* (Fig. 3D). This favors a role for InsPs rather than for P_i in AtPHO1-mediated plant P_i homeostasis. The ΔN15 mutant phenotype underlines the importance of helix α1 in SPX domain function, further supporting the idea of an InsP-induced conformational change (Fig. 3D). Shoot P_i content in PBC, KSC and ΔN15 plants was reduced compared to wild-type, and similar to *pho1* plants, suggesting that P_i export into the xylem is compromised in these mutants (Fig. 3E). Expression of P_i starvation-induced genes was up-regulated in shoots of PBC, KSC and ΔN15 mutant lines, to an even larger extent when compared to *pho1* knock-out plants (Fig. 3F). Targeting the ligand-binding function of SPX^{AtPHO1} thus impairs P_i export and enhances P_i starvation signaling in the P_i-deficient *pho1* mutant. P_i efflux was also found impaired in patients with brain calcification carrying mutations in SPX^{HsXPR1}, indicating that InsP control of P_i transport is conserved across evolution (Fig. S11) (*24*).

In our SPX-$InsP_6$ complexes one ligand face remains accessible for additional coordination by target proteins (Fig. 2C-F), which may serve as co-receptors for InsP signaling molecules, similarly as

observed for the plant jasmonate receptor (*25*) or for the cyclin-dependent kinase complex Pho80 – Pho85 and its inhibitor Pho81 (*26*). SPX proteins from rice interact with the OsPHR2 transcription factor in the presence of 15 mM P_i (*16, 27*). We found that OsSPX4 and OsPHR2 interact at 5-$InsP_7$ concentrations as low as 20 μM (Fig. 4A). No significant binding was detected in calorimetry experiments upon titrating P_i, PP_i, PPP_i or ATP into a 1:1 OsSPX4/OsPHR2 protein solution (Figs. 4B, S12). $InsP_6$ bound with a K_d of ~50 μM, whereas 5-$InsP_7$ bound with ~7 μM affinity. In contrast to SPX^{ScVtc2}, the OsSPX4 – OsPHR2 complex can thus sense the presence of the pyrophosphate group, indicating that interacting proteins may assist SPX domains in selective InsP recognition (Figs. 2B, 4B, S12) (*4, 13, 15, 16*). $InsP_6$ binding was disrupted in the OsSPX4 PBC triple mutant, again suggesting that the basic surface cluster contributes to InsP sensing. Finally, we titrated OsSPX4 into a solution containing OsPHR2 pre-incubated with a 2-fold molar access of 5-$InsP_7$. We observed formation of a 1:1 SPX domain – transcription factor complex with a dissociation constant of ~15 μM, whereas in the absence of InsPs no binding occurred (Fig. 4B). Thus, InsPs can promote the specific interaction of plant SPX proteins with their transcription factor targets. Given that the P_i concentration in the plant cytosol may not exceed 100 μM, InsPs but not P_i itself should represent physiological ligands for plant SPX proteins (*28, 29*). This would explain why Arabidopsis $InsP_5$ kinase mutants, which contain less than normal $InsP_6$ and PP-InsPs (*19*), but have higher cellular P_i, nonetheless show constitutive P_i starvation responses (*30*).

Our crystallographic, biochemical and genetic analysis of fungal, plant and human SPX domain-containing proteins suggests that these domains function as cellular receptors for InsP signaling molecules (*19*). In our assays, the PP-InsP 5-$InsP_7$ activates the yeast VTC complex and promotes association between SPX proteins and transcription factors in plants. Importantly, $InsP_7$ levels decrease under P_i starvation in yeast (*18*) (Table S4). PP-InsPs may thus signal the cellular P_i status by binding to SPX domains in P_i-sufficient conditions, enabling them to interact with a multitude of proteins that regulate P_i homeostasis in eukaryotic cells (*4, 13, 15, 16, 27*). We speculate that the highly plastic basic binding surface may allow SPX domains to sense different InsP/PP-InsP isomers, which could convey signaling inputs from various physiological processes (*19*). Our work now opens venues for specifically manipulating InsP/PP-InsP signaling in eukaryotic cells to uncover additional interaction partners for SPX domains. The P_i signaling pathways we have studied here may prove useful for engineering phosphate use efficiency in crop plants.

References and Notes:

1. M. Lenburg, E. O'Shea, *Trends Biochem. Sci.* **21**, 383–387 (1996).
2. T.-J. Chiou, S.-I. Lin, *Annu. Rev. Plant Biol.* **62**, 185–206 (2011).
3. D. Secco *et al.*, *New Phytol.* **193**, 842–851 (2012).
4. H. C. Hürlimann, B. Pinson, M. Stadler-Waibel, S. C. Zeeman, F. M. Freimoser, *EMBO Rep.* **10**, 1003–1008 (2009).
5. D. Hamburger, E. Rezzonico, J. MacDonald-Comber Petétot, C. Somerville, Y. Poirier, *Plant Cell*. **14**, 889–902 (2002).
6. J. Liu *et al.*, *Proc. Natl. Acad. Sci. U. S. A.* **112**, E6571–8 (2015).
7. D. Giovannini, J. Touhami, P. Charnet, M. Sitbon, J.-L. Battini, *Cell Rep.* **3**, 1866–1873 (2013).
8. M. Hothorn *et al.*, *Science*. **324**, 513–516 (2009).
9. N. Ogawa *et al.*, *Mol. Cell. Biol.* **15**, 997–1004 (1995).
10. B. S. Park, J. S. Seo, N.-H. Chua, *Plant Cell*. **26**, 454–464 (2014).
11. K. Duan *et al.*, *Plant J.* **54**, 965–975 (2008).
12. S. Wege *et al.*, *Plant Physiol.* **170**, 385–400 (2016).
13. D. D. Wykoff, A. H. Rizvi, J. M. Raser, B. Margolin, E. K. O'Shea, *Mol. Cell*. **27**, 1005–1013 (2007).
14. V. Rubio *et al.*, *Genes Dev.* **15**, 2122–2133 (2001).
15. M. I. Puga *et al.*, *Proc. Natl. Acad. Sci. U. S. A.* **111**, 14947–52 (2014).
16. Z. Wang *et al.*, *Proc. Natl. Acad. Sci. U. S. A.* **111**, 14953–8 (2014).
17. L. Holm, S. Kääriäinen, P. Rosenström, A. Schenkel, *Bioinformatics*. **24**, 2780–2781 (2008).
18. A. Lonetti *et al.*, *J. Biol. Chem.* **286**, 31966–31974 (2011).
19. S. B. Shears, *Adv. Biol. Regul.* **57**, 203–216 (2015).
20. C. Auesukaree, H. Tochio, M. Shirakawa, Y. Kaneko, S. Harashima, *J. Biol. Chem.* **280**, 25127–25133 (2005).
21. M. A. Lemmon, K. M. Ferguson, C. S. Abrams, *FEBS Lett.* **513**, 71–76 (2002).
22. N. Ogawa, J. DeRisi, P. O. Brown, *Mol. Biol. Cell*. **11**, 4309–4321 (2000).
23. S. Wege *et al.*, *Plant Physiol.* (2015), doi:10.1104/pp.15.00975.
24. A. Legati *et al.*, *Nat. Genet.* **47**, 579–81 (2015).
25. L. B. Sheard *et al.*, *Nature*. **468**, 400–405 (2010).
26. Y.-S. Lee, S. Mulugu, J. D. York, E. K. O'Shea, *Science*. **316**, 109–112 (2007).
27. Q. Lv *et al.*, *Plant Cell*. **26**, 1586–97 (2014).
28. J. Pratt *et al.*, *Plant Physiol.* **151**, 1646–1657 (2009).
29. M. Desai *et al.*, *Plant J.* **80**, 642–653 (2014).
30. J. Stevenson-Paulik, R. J. Bastidas, S.-T. Chiou, R. A. Frye, J. D. York, *Proc. Natl. Acad. Sci. U. S. A.* **102**, 12612–12617 (2005).

Acknowledgments: We thank G. Bräunlich for help with data analysis and J. Piehler for a sample of tris-NTA-Oregon Green488. Atomic coordinates and structure factors have been deposited with the Protein Data Bank with accession numbers 5IIG (SPX-TTM^{ScVtc4} form A), 5IIQ (SPX-TTM^{ScVtc4} form B), 5IIT (SPX^{ScVtc4}-macro), 5IJH (SPX^{HsXPR1} SO_4^{2-}), 5IJJ (SPX^{CtGde1} $InsP_6$) and 5IJP (SPX^{CtVtc4} $InsP_6$). We thank Stefanie Wege for assistance with confocal microscopy and P_i export assays. This project was funded by grants from the European Research Council under the European Union's Seventh Framework Programme (FP/2007-2013) / ERC Grant Agreement n. 310856, the European Molecular Biology Organisation (EMBO) Young Investigator Programme (to M.H.), the Swiss National Fund 31003A-138339 and 31003A-159998 (to Y.P.), an SNF Professorship PP00P2 157607 (to H.J.J.), and from ERC Grant n. 233458 and SNF grant 144258 (to A.M.). Diffraction experiments were performed at beam lines PXII and PXIII of the Swiss Light Source, Paul Scherrer Institute, Villigen and at beam-line ID29 of the European Synchrotron Radiation Facility, Grenoble, France. Supplement contains additional data.

Fig. 1. SPX helical bundles provide a positively charged ligand binding surface. (**A**) Ribbon diagram of apo SPX^{ScVtc4} with core helices in blue and surrounding helices colored from N- to C-terminus in yellow to red. (**B**) Ribbon diagrams of the reductively methylated SPX^{ScVtc4} (left), SPX^{CtGde1} (middle) and of SPX^{HsXPR1} (right) shown in two orientations (colors as in A). (**C**) Electrostatic surface potential of the SPX domains from (B) reveals the SPX basic surface cluster. (**D**) A sulfate ion is bound to the SPX^{HsXPR1} basic surface cluster. Interacting residues are shown in bonds representation (PBC, in bold; KSC; in italics), a distant Lys residue (SC) is shown alongside. Residue numbers correspond to SPX^{HsXPR1} (SPX^{ScVtc2} in brackets). (**E**) Table summaries for NMR titrations of wild-type and mutant SPX^{ScVtc2} and SPX^{HsXPR1} with different candidate ligands.

Fig. 2. SPX domains sense InsP signaling molecules. (**A**) VTC-dependent polyP synthesis by isolated yeast vacuoles in response to increasing concentrations of externally supplied P_i, SO_4^{2-}, $InsP_6$ and 5-$InsP_7$. (**B**) Binding affinities of different SPX domains vs. 5-$InsP_7$ and $InsP_6$ by isothermal titration calorimetry and microscale thermophoresis (indicated by an*) (± fitting errors). (**C**) Ribbon diagram of SPX^{CtGde1} in complex with $InsP_6$ (in bonds representation, colors as in Fig. 1A) and including a $2F_o - F_c$ omit electron density map contoured at 1.5 σ. (**D**) Close-up view of the SPX^{CtGde1} with $InsP_6$ – protein interactions depicted as dotted lines. (**E**) Ribbon diagram and close up view of the SPX^{CtVtc4} – $InsP_6$ complex. (**F**) Rotated view of the SPX^{CtVtc4} complex highlighting the interactions of $InsP_6$ with main-chain atoms of helix α1.

Fig. 3. Mutations in the SPX InsP-binding site affect polyP synthesis in yeast and plant P_i transport and P_i starvation signaling. (**A**) Isothermal titration calorimetry of wild-type and of PBC and KSC mutant SPX^{ScVtc2} vs. $InsP_6$ (± fitting errors). (**B**) Table summaries of the conserved surface cluster residues in the different SPX-domain containing proteins used in this study. (**C**) PolyP synthesis by isolated vacuoles carrying VTC complexes with corresponding substitutions in the SPX basic surface clusters of subunits Vtc3 and Vtc4 and in the presence or absence of 0.5 µM 5-$InsP_7$. (**D**) Shoot phenotypes of 28-d-old T2 *pho1-2* transgenic lines, carrying promPHO1::PHO1:GFP (labeled wild-type) or its mutant variants. (**E**) Shoot P_i content of the transgenic lines from D. (**F**) Normalized relative expression of selected P_i-starvation induced genes in the different *pho1-2* complementation lines.

Fig. 4. InsPs trigger the association of plant SPX proteins with PHR transcription factors. (**A**) *In vitro* pull-down of full-length OsSPX4 containing a C-terminal HA-tag. Interaction with full-length untagged OsPHR2 in the presence of either 20 µM 5-$InsP_7$ or P_i, respectively. (**B**) Isothermal titration calorimetry of OsSPX4/OsPHR2 vs. different ligands (5-$InsP_7$, black; $InsP_6$, dark-blue; 1,3,4,5,6-$InsP_5$, magenta; OsSPX4-PBC mutant vs. $InsP_6$, light-blue) and including table summaries for different titrations (± fitting errors, n.d. no detectable binding). The * indicates experiments performed by microscale thermophoresis.

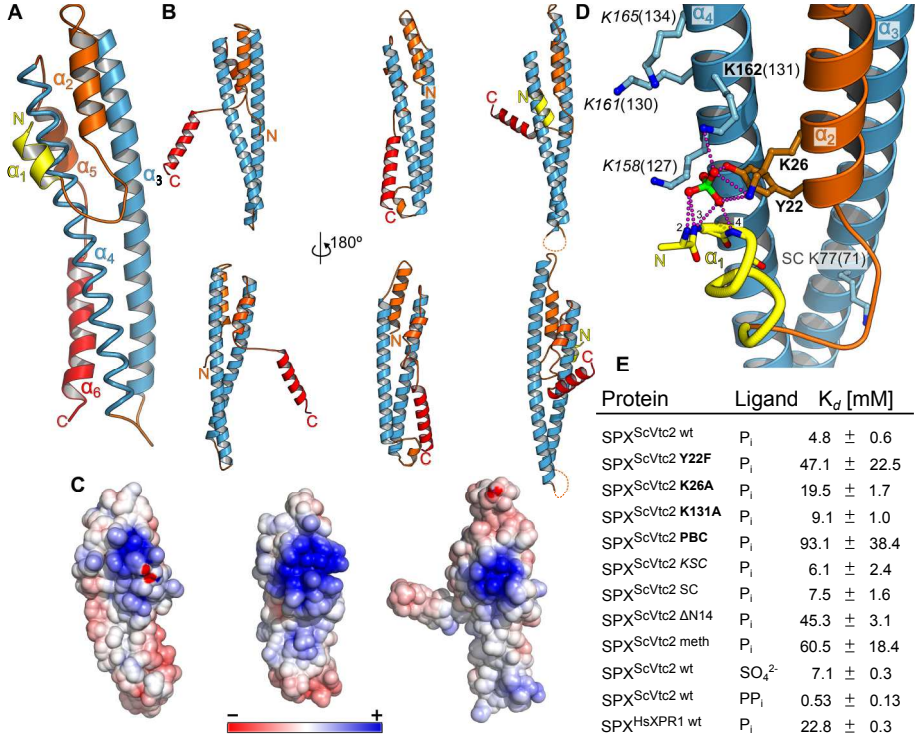

Protein	Ligand	K_d [mM]
$SPX^{ScVtc2\ wt}$	P_i	4.8 ± 0.6
$SPX^{ScVtc2\ \mathbf{Y22F}}$	P_i	47.1 ± 22.5
$SPX^{ScVtc2\ \mathbf{K26A}}$	P_i	19.5 ± 1.7
$SPX^{ScVtc2\ \mathbf{K131A}}$	P_i	9.1 ± 1.0
$SPX^{ScVtc2\ \mathbf{PBC}}$	P_i	93.1 ± 38.4
$SPX^{ScVtc2\ KSC}$	P_i	6.1 ± 2.4
$SPX^{ScVtc2\ SC}$	P_i	7.5 ± 1.6
$SPX^{ScVtc2\ \Delta N14}$	P_i	45.3 ± 3.1
$SPX^{ScVtc2\ meth}$	P_i	60.5 ± 18.4
$SPX^{ScVtc2\ wt}$	SO_4^{2-}	7.1 ± 0.3
$SPX^{ScVtc2\ wt}$	PP_i	0.53 ± 0.13
$SPX^{HsXPR1\ wt}$	P_i	22.8 ± 0.3

Fig. 1. (Wild *et al*.) (120x96 mm)

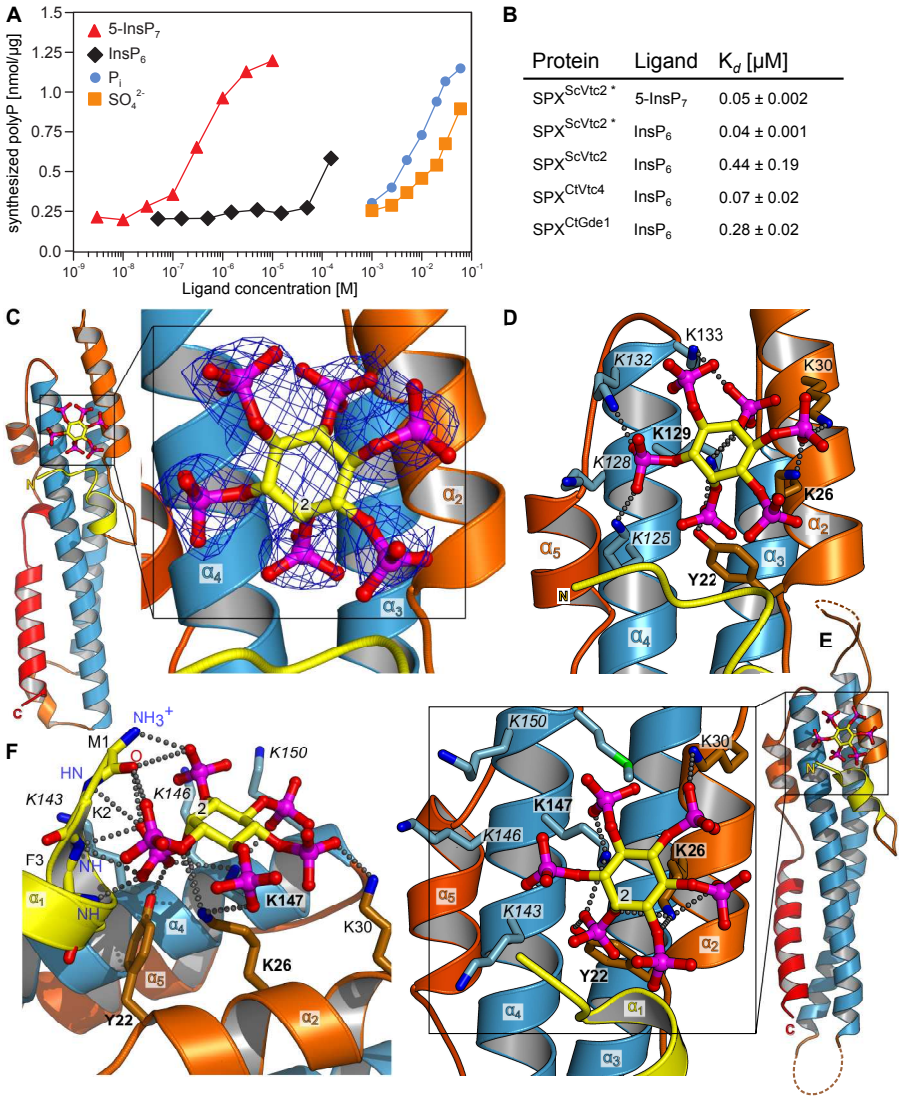

Protein	Ligand	K_d [µM]
$SPX^{ScVtc2*}$	5-$InsP_7$	0.05 ± 0.002
$SPX^{ScVtc2*}$	$InsP_6$	0.04 ± 0.001
SPX^{ScVtc2}	$InsP_6$	0.44 ± 0.19
SPX^{CtVtc4}	$InsP_6$	0.07 ± 0.02
SPX^{CtGde1}	$InsP_6$	0.28 ± 0.02

Fig. 2. (Wild *et al.*) (118x144 mm)

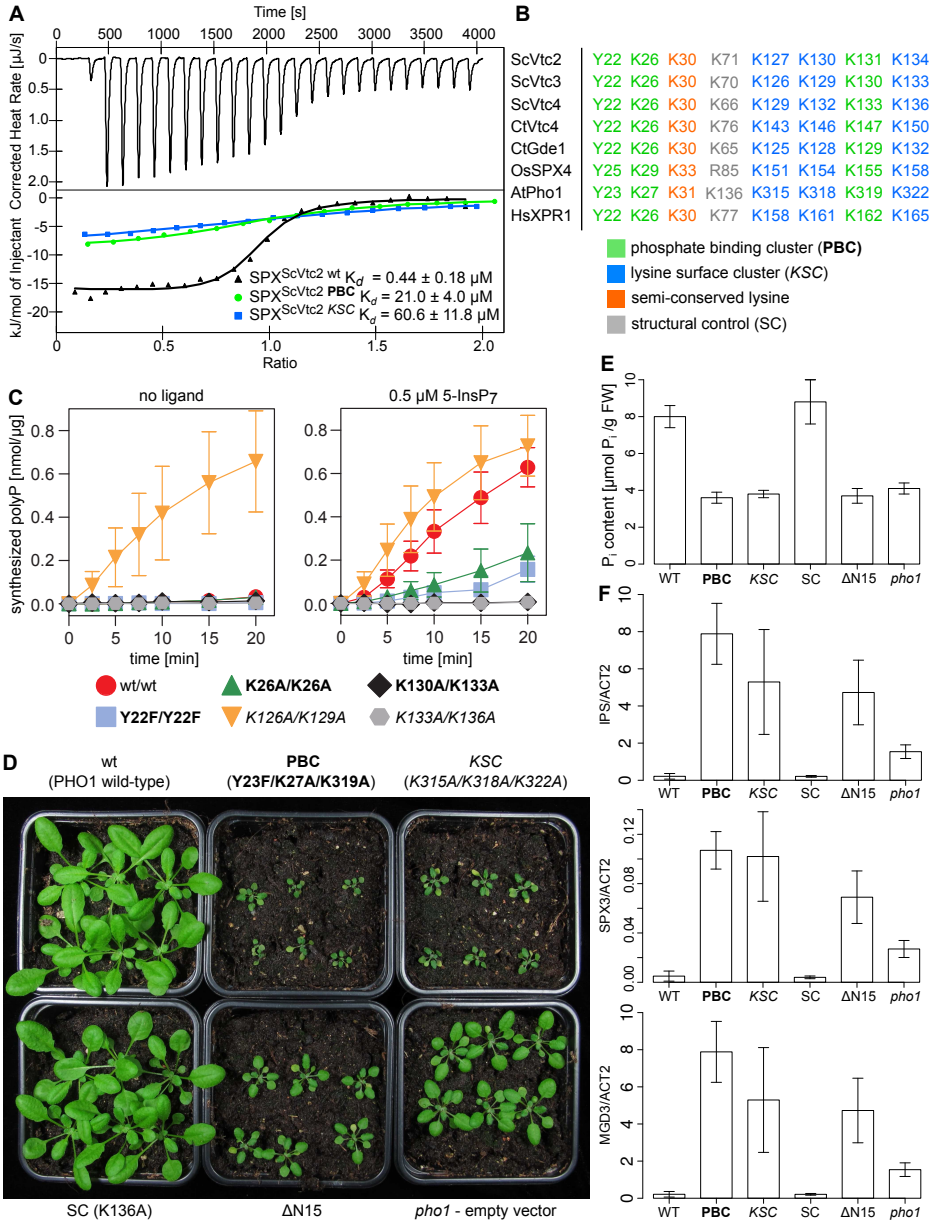

Fig. 3. (Wild *et al.*) (120x160 mm)

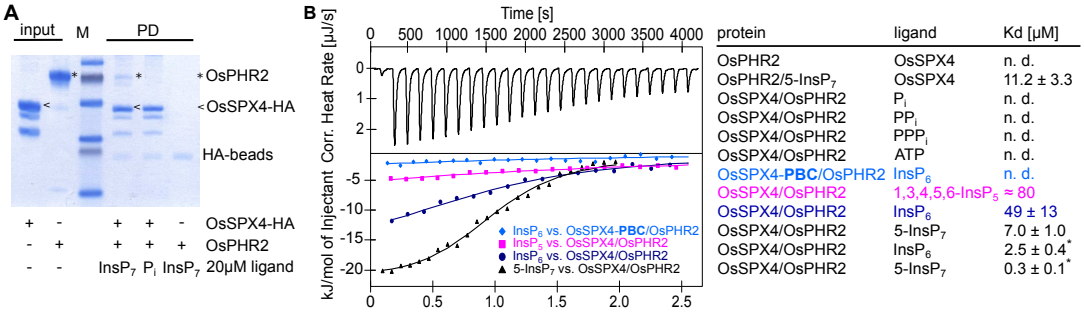

protein	ligand	Kd [µM]
OsPHR2	OsSPX4	n. d.
OsPHR2/5-$InsP_7$	OsSPX4	11.2 ± 3.3
OsSPX4/OsPHR2	P_i	n. d.
OsSPX4/OsPHR2	PP_i	n. d.
OsSPX4/OsPHR2	PPP_i	n. d.
OsSPX4/OsPHR2	ATP	n. d.
OsSPX4-**PBC**/OsPHR2	$InsP_6$	n. d.
OsSPX4/OsPHR2	1,3,4,5,6-$InsP_5$	≈ 80
OsSPX4/OsPHR2	$InsP_6$	49 ± 13
OsSPX4/OsPHR2	5-$InsP_7$	7.0 ± 1.0
OsSPX4/OsPHR2	$InsP_6$	2.5 ± 0.4*
OsSPX4/OsPHR2	5-$InsP_7$	0.3 ± 0.1*

Fig. 4. (Wild *et al*.) (142x40 mm)

Supplementary Materials for

Control of Eukaryotic Phosphate Homeostasis by inositol polyphosphate sensor domains.

Rebekka Wild, Ruta Gerasimaite, Ji-Yul Jung, Vincent Truffault, Igor Pavlovic, Andrea Schmidt, Adolfo Saiardi, Henning Jacob Jessen, Yves Poirier, Michael Hothorn, Andreas Mayer

correspondence to: yves.poirier@unil.ch, michael.hothorn@unige.ch, andreas.mayer@unil.ch

This PDF file includes:

Materials and Methods
Supplementary Text
Supplementary References 31-54
Figs. S1 to S14
Tables S1 to S4

Materials and Methods

Protein expression and purification

A catalytically inactive portion of VTC subunit ScVtc4 comprising the N-terminal SPX and polyP-synthesizing triphosphate tunnel metalloenzyme (TTM) domains (*8*, *31*), SPX – TTM^{ScVtc4} (1−480) and containing a catalytic TTM point mutation (Glu426 → Asn) (*8*) was cloned into the pMH-HT providing a tobacco etch virus (TEV) cleavable N-terminal 6xHis tag. For carrier driven crystallization, SPX^{ScVtc4} (1−178) was combined with the human histone macroH2A1.1 macro domain (*32*) at the C-terminus, connected via a three amino acid linker (Ala-Gly-Ser) and resulting in a stable SPX^{ScVtc4} – macro fusion protein. SPX^{ScVtc2} (residues 1−182), SPX^{HsXPR1} (1−207), SPX^{CtVtc4} (1-193) and SPX^{CtGde1} (1-184) were cloned into a modified pET vector (pMH-HC), providing a C-terminal 6xHis tag. Full-length of OsSPX4 and OsPHR2 were cloned into vector pMH-HSsumo, provided a N-terminal sumo fusion protein and 8xHis-Strep tandem affinity tags. Site specific mutations including the triple PBC and KSC mutations were introduced by PCR and verified by sequencing. Proteins were recombinantly expressed in *E. coli* BL21 (DE3) RIL cells using terrific broth medium. Reductive protein methylation of SPX^{ScVtc4} – macro was performed as described (*33*). For NMR experiments bacteria were grown in minimal medium containing $^{15}NH_4Cl$ as the only nitrogen source. Cells were grown to OD_{600nm} = 0.6 at 37 ºC. The temperature was reduced to 16 ºC and protein expression was induced with 0.3 mM isopropyl β-D-galactoside (IPTG) for 16 h. Cells were harvested by centrifugation for 20 min at 4,500 xg at 4 ºC, washed with PBS and snap-frozen in liquid nitrogen. For protein purification cells were re-suspended in lysis buffer (50 mM Tris/HCl pH 7.8, 500 mM NaCl, 2 mM β-mercaptoethanol [β-ME], 0.1 % (v/v) IGEPAL, 1 mM $MgCl_2$, 500 units TurboNuclease (BioVision), 2 tablets Protease Inhibitor Cocktail (Roche)) and lysed with an EmulsiFlex-C3 (Avestin). Lysates were cleared by centrifugation at 7,000 xg and 4 ºC for 1 h. The supernatant was loaded onto a 5 mL HisTrap HP Ni^{2+} affinity column (GE Healthcare). Columns were washed with 5 column volumes (CV) of lysis buffer, 5 CV phosphate buffer (200 mM KH_2PO_4 /K_2HPO_4, pH 7.8, 2 mM β-ME), 5 CV of high salt buffer (50 mM Tris/HCl pH 7.8, 1 M NaCl, 2

mM β-ME) followed by 2 CV of lysis buffer. Purified SPX domain proteins eluted on a step gradient against lysis buffer supplemented with 250 mM imidazole, pH 8.0. Cleavable N-terminal 6xHis tags were removed by adding recombinant TEV protease at 1:100 molar ratio for 16 h at 4 ºC. The tag and the 6xHis-tagged TEV protease were removed in a subsequent second Ni^{2+} affinity step. The Sumo-fusion tag was removed by addition of Sumo protease and the 8xHis tagged fusion tag was separated from OsSPX4 and OsPHR2 protein samples by a second Ni^{2+} chomatography step. Proteins were dialyzed against size-exclusion chromatography (SEC) buffer (20 mM Hepes/NaOH pH 7.0, 300 mM NaCl, 0.5 mM TCEP) for 16 h at 4 ºC. Samples were loaded onto a Superdex 75 HR26/60 column (GE healthcare) and monomeric peak fractions were pooled and concentrated. Purified proteins were snap-frozen in liquid N_2 and stored at -80 ºC.

Crystallization and data collection

Crystals of ScVtc4 SPX-TTM form A developed at room temperature in hanging drops composed of 1.5 µL of protein solution (4.5 mg/mL in 20 mM Hepes/NaOH pH 7.0, 250 mM NaCl, 1 mM EDTA, 0.5 mM tris(2-carboxyethyl)phosphine (TCEP)) and 1.5 µL crystallization buffer (1.5 M Li_2SO4, 0.1 M Hepes/NaOH pH 7.5) suspended over 0.4 mL of the latter as reservoir solution. Crystals were transferred into reservoir solution supplemented with 15 % (v/v) glycerol by serial transfer and snap frozen in liquid nitrogen. Hexagonal crystals (form B) were grown at a protein concentration of 1.2 mg/mL in 1.5 M $(NH_4)_2SO_4$, 4 % PEG 1,000, 0.1 M Hepes/NaOH pH 7.5 and cryo-protected by addition of glycerol to a final concentration of 25 % (v/v). Both crystal forms diffracted to about 3 Å resolution at beam-lines PXII/III of the Swiss Light Source (SLS), Villigen, Switzerland. A structure of isolated SPX^{ScVtc4} was obtained by carrier-driven crystallization with the macro domain of human histone macroH2A1.1 from reductively methylated protein samples (10 mg/mL in 20 mM Hepes/NaOH pH 6.5, 300 mM NaCl, 0.5 mM TCEP). The SPX-macro fusion protein crystallized in 19 % (v/v) PEG 3,350, 0.1 M $(NH_4)_2SO_4$, 0.1 M Mes/NaOH pH 6.5. Crystals were transferred to crystallization buffer containing 15 % (v/v) glycerol for cryo-protection and diffracted to 2.13 Å at beam-line ID29 of the European Synchrotron Radiation Facility (ESRF),

Grenoble, France. Next, crystals of SPX^{HsXPR1} (5 mg/mL in 20 mM Hepes/NaOH pH 7.0, 275 mM NaCl, 0.5 mM EDTA) appeared in 1.4 M $(NH_4)_2SO_4$, 16 % (v/v) glycerol, 0.1 M Tris/HCl pH 8.5 and were cryoprotected by adding glycerol to a final concentration of 30 % (v/v). The SPX^{HsXPR1} crystal lattice is stabilized by an inter-molecular disulfide bond, yielding a data set at 2.43 Å at ESRF beam-line ID29. A high resolution $InsP_6$ complex was obtained from crystals of SPX^{CtGde1} (13.5 mg/mL, 20 mM Hepes/NaOH pH 7.0, 200 mM NaCl, 0.25 TCEP, 10 mM $InsP_6$) grown from hanging drops containing 25 % (v/v) PEG 3,350, 0.1 M $(NH_4)_2Ac$, 0.1 M Bis-Tris/HCl pH 6.5; diffracting to 1.95 Å at SLS PXIII after cryo-protection by serial transfer into crystallization buffer containing 25 % (v/v) ethylene glycol. The *C. thermophilum* orthologue of ScVtc4 yielded diffracting crystals in complex with $InsP_6$: SPX^{CtVtc4} at 10 mg/mL in 20 mM Hepes/NaOH pH 7.0, 200 mM NaCl, 0.25 mM TCEP, 10 mM $InsP_6$ crystallized in 13 % PEG (v/v) 3,350, 6 % (v/v) Tacsimate pH 5.0. Glycerol to a final concentration of 15 % (v/v) was added directly to the crystallization drop for cryo-protection. A highly redundant data set to 2.75 Å was collected along a needle-shaped crystal at SLS beam-line PXIII. Data processing and scaling were done in XDS (*34*).

Crystallographic structure solution and refinement

The structures of ScVtc4 SPX-TTM and SPX-macro were solved using the molecular replacement method as implemented in the program PHASER (*35*) and using the previously determined TTM (PDB-ID 3g3r) and macro1.1 (PDB-ID 1zr3) structures as search models. PHASER solved the structures of SPX^{HsXPR1}, SPX^{CtVtc4} and SPX^{CtGde1}, when given the conserved SPX^{ScVtc4} α4 and α5 core helices as search models. The structures were completed in alternative cycles of manual model building in COOT (*36*) and restrained TLS refinement in autoBUSTER (Global Phasing Limited). Analysis with MolProbity (*37*) indicates excellent stereochemistry for all refined models. Refinement statistics are summarized in Table S1. Structural representations were done in POVSCRIPT+ (*38*) and rendered with the program POVRAY (http://www.povray.org). Electrostatic surface potentials were calculated with the program APBS (*39*) and mapped onto molecular surfaces calculated with MSMS (*40*).

NMR binding assays

From all proteins tested, only SPX^{ScVtc2} and SPX^{HsXPR1} were suitable for NMR experiments. We could only synthesize limited amounts of 5-$InsP_7$ and thus we used $InsP_6$, a commercially available InsP, as substitute in our binding studies and in our crystallization screens. For NMR experiments ^{15}N-labeled SPX^{ScVtc2} wild type, as well as the PBC, KSC and single point mutants were purified and concentrated to 10 mg/mL in NMR buffer (25 mM Hepes/NaOH pH 7.0, 250 mM NaCl, 1 mM EDTA, 0.5 mM TCEP) and 50 µL D_2O were added to 450 µL protein solution. The ΔN14 mutant was less stable in our hands. For NMR titrations a 2.5 M Na_2HPO_4 / NaH_2PO_4 stock solution at pH 7.0 was prepared and added to the sample to obtain final P_i concentrations of 0, 1.5, 5, 10, 20, 40 and 100 mM. Similar concentrations were used for the Na_2SO_4 and sodium PP_i titrations. $InsP_6$ was added to final concentrations of 0, 0.025, 0.075, 0.2, 0.4 and 1 mM, respectively. We found several corresponding peak shifts in our $InsP_6$ and P_i titrations, suggesting that P_i and $InsP_6$ may occupy partially overlapping binding sites in SPX. This was later confirmed by our complex crystal structures. All spectra were recorded at 298 K at 600 MHz on a Bruker AVIII-600 spectrometer. To confirm the oligomeric purity of the samples under the conditions of the NMR experiments the molecular diffusion coefficient for the protein was measured prior to every ligand binding experiments. For the ligand titration experiments, efb-^{15}N-HSQC spectra of [U-^{15}N] SPX^{ScVtc2} in the absence and presence of the ligands were recorded (*41*). ^{1}H-^{15}N-HSQC spectra were recorded with 128(F1) 1024(F2) complex data points and spectral widths of 3650 Hz (F1) 7812 Hz (F2). 8 or 24 scans were used per increment with an inter-scan delay of 0.6 s. Spectra processing was done using TopSpin 2.1 (Bruker) where a zero filling to 256(F1) was applied. Spectra analysis was performed with Sparky 3.115. Chemical shift perturbations (CSP) were calculated using the equation

$$CSP_{\text{obs}} = \sqrt{\frac{\left(\frac{\Delta\delta_N}{5}\right)^2 + (\Delta\delta_H)^2}{2}}$$

, where $\Delta\delta_H$ and $\Delta\delta_N$ are the chemical shifts difference for the ^{1}H and ^{15}N resonances, respectively. Dissociation constants (K_d) were determined by fitting the data to a function described by

$$CSP_{\text{obs}} = CSP_{\max} \cdot \frac{K_d - [L] + [P] - \sqrt{(K_d + [L] + [P])^2 - 4[P][L]}}{2[P]}$$

, where [L] is the ligand concentration, [P] the protein concentration and CSP_{max} the maximal chemical shift between the protein in bound and unbound state.

Chemical synthesis and analysis of 5-$InsP_7$

^{1}H-NMR spectra were recorded on a Bruker 400 MHz spectrometer at 298K in the indicated deuterated solvent. Data are reported as follows: chemical shift (δ, ppm), multiplicity (s, singulet; d, doublet; t, triplet; q, quartet; m, multiplet or not resolved signal; br, broad signal), coupling constant(s) (J, Hz), integration. All signals were referenced to the internal solvent signal as standard ($CDCl_3$, δ 7.26; D_2O, δ 4.79; CD_3OD, δ 3.31; DMSO-d6, δ 2.50). ^{31}P[^{1}H]-NMR spectra and ^{31}P-NMR spectra were recorded with ^{1}H-decoupling or ^{1}H coupling on Bruker 162 MHz or 202 MHz spectrometers at 298K in the indicated deuterated solvent. All signals were referenced to an internal standard (PPP). ^{13}C[^{1}H]-NMR spectra were recorded with ^{1}H-decoupling on Bruker 101 or 125 MHz spectrometers at 298K in the indicated deuterated solvent. All signals were referenced to the internal solvent signal as standard ($CDCl_3$, δ77.0; CD_3OD, δ 49.0; DMSO-d6, δ 39.5). Mass spectra were recorded spectroscopy on Finnigan MAT95 MS, Bruker EsquireLC MS, Bruker maXis QTof HR MS and Finnigan TSQ700 MS machines. The chemical synthesis is outlined in Fig. S13, analytical data can be found in Fig. S14.

Synthesis of phosphate triester 1

The compound was synthesized as described before in four steps starting from myo-inositol. Analytical data were identical with the values reported in the literature (*42*).

Synthesis of protected hexakisphosphate 2

100 mg (0.27 mmol, 1.0 eq.) monophosphate ester **1** and 656 mg (2.46 mmol, 9 eq.) o-xylylene *N,N*-di*iso*propylamino phosphoramidite (Xe-PA) were coevaporated with dry MeCN (2 mL). The residue was dissolved in dry MeCN (2 mL) and dry DMF (1 mL). To this solution 290 mg (2.46 mmol, 9 eq.) DCI was added. Progress of the reaction was monitored by ^{31}P-NMR. After completion of the reaction (15 min), oxidation was achieved by slow addition of 424 mg (2.46 mmol, 9 eq.) *m*CPBA (70% moistened with

water) at 0ºC. The reaction mixture was concentrated in vacuo. The product was purified by FC (gradient: EtOAc to EtOAc/MeOH 20:1) yielding 325 mg of **2** as a colorless oil (0.254 mmol, 93 %). ^{1}H NMR (400 MHz, 298K, $CDCl_3$, δ/ppm): 7.34 - 7.16 (m, 20H), 5.71 - 5.50 (m, 4H), 5.47 - 5.29 (m, 5H), 5.23 - 4.96 (m, 15H), 4.86 (dd, *J* = 11.5, 9.0 Hz, 1H), 4.45 - 4.22 (m, 4H), 3.60 (d, *J* = 12.0 Hz, 1H), 2.84 - 2.63 (m, 4H); ^{31}P{^{1}H}NMR (162 MHz, 298K, $CDCl_3$, δ/ppm): -1.39 , -2.20 , -2.57 , -3.11; ^{31}P NMR (162 MHz, 298K, $CDCl_3$, δ/ppm): -1.05- -1.73 (m), -1.93- -2.41 (m), -2.41- -2.87 (m), -2.89- -3.36 (m); R_f (SiO_2, EtOAc:MeOH; 8:1) 0.5; HRMS (ESI) calcd. for $C_{52}H_{54}N_2Na_2O_{24}P_6$ [$(M+2Na)^{2+}$] 661.0638, found 661.0633.

Synthesis of protected 5-InsP$_7$ 3

Hexakisphosphate **2** 117 mg (0.092 mmol, 1.0 eq.) was dissolved in dry MeCN (2 mL). 48 µL (0.367 mmol, 4.0 eq.) of DBU were added followed by addition of 84 µL (0.37 mmol, 4.0 eq.) BSTFA (*N,O*-Bis(trimethylsilyl)trifluoroacetamide). The solution was stirred 15 minutes at room temperature. The reaction was monitored by TLC. After completion of the deprotection, 85 µL (0.37 mmol, 4.0 eq.) MeOH and 25 µL (0.37 mmol, 4.0 eq.) TFA were added to the solution. The mixture was stirred for 10 min and then evaporated to dryness. The residue was taken up in dry MeCN (2 mL), 64 mg (0.18 mmol, 2.0 eq.) of bis-benzyl *N,N*-di*iso*propylamino phosphoramidite and 430 µL (0.45 M in MeCN, 0.182 mmol, 2.0 eq.) 1*H*-tetrazole were added. The solution was stirred for 15 minutes at room temperature and then cooled down (0 °C). Progress of the reaction was monitored by ^{31}P NMR. After completion of the reaction, oxidation was achieved by slow addition of 32 mg (0.18 mmol, 2.0 eq.) *m*CPBA (70% moistened with water). MeCN was removed almost to dryness and product was precipitated from Et_2O (overnight at 4ºC). The isolated product was dried *in vacuo* to yield (85 mg, 0.053 mmol, 58 %). The product can be additionally purified by RP-18 chromatography (water/MeOH 3:1 – 1:2 v/v). ^{1}H NMR (400 MHz, 298 K, $CDCl_3$, δ/ppm): 10.61 (s, DBU), 7.32 - 7.04 (m, 28H), 6.98 (m, 2H), 5.79 - 4.73 (m, 30H), 4.03 (m, DBU), 3.31 - 2.97 (m, DBU), 2.58 (s, 1H), 1.95 (s, DBU), 1.73 - 1.08 (m, DBU); ^{31}P{^{1}H}NMR (162 MHz, 298 K, $CDCl_3$, δ/ppm): -1.94 , -2.61 , -10.68 (d, *J* = 13.6 Hz), -12.40 (d, *J* = 14.0 Hz); ^{31}P NMR (162 MHz, 298 K, $CDCl_3$, δ/ppm): -1.37 - -2.27 (m), -2.27 - -3.16 (m), -10.10 - -11.05 (m), -12.40 (dd, *J* =

12.6 Hz, 12.6 Hz); R_f (SiO_2, DCM:MeOH; 8:1): 0.3; HRMS (ESI) calculated for $C_{60}H_{60}O_{27}P_7$ (M^-) 1429.1491, found 1429.1509.

Synthesis of 5-InsP$_7$ 4

The reactions can be either conducted in a stainless steel autoclave with a Teflon inlet at 80 bar H_2 (2-3 hours) or in a Parr apparatus at 4 bar H_2 (6-7 hours). 15 mg (9.5 μmol, 1.0 eq.) of protected 5-PP-InsP$_5$ **3** were dissolved in a mixture of *t*-BuOH and water (4:1, 10 mL) and 8.8 mg (0.095 mmol, 11 eq.) $NaHCO_3$ and 14 mg Pd/black (143 μmol, 13 eq.) were added to the solution. The reaction mixture was then stirred for 4 h under H_2 (4 bar) and then water (22 mL) was added. The hydrogenation was continued for 2.5 more hours. The catalyst was removed by centrifugation, washed with water and the combined aqueous layers were freeze-dried. Crystallization of the residue from water/acetone yielded 5-PP-InsP$_5$ **4** as a colorless solid in the sodium form (6.2 mg, 8.37 μmol, < 88% Maximal yield was calculated for completely protonated species M = 740.01; Minimal yield > 64% (6.04 μmol) for 13 Na^+; M = 1025.78, sodium salt with unknown amount of counter ions.). ^{1}H NMR (500 MHz, 298 K, deuterium oxide, δ /ppm): 4.82 (dd, *J* = 9.8 Hz, *J* = 9.8 Hz, ^{1}H), 4.48 (ddd, *J* = 9.5 Hz, *J* = 9.5 Hz, *J* = 9.5 Hz, ^{1}H), 4.45 (ddd, *J* = 9.5 Hz, *J* = 9.5 Hz, *J* = 9.5 Hz, ^{1}H) 4.25 (dd, *J* = 9.5 Hz, *J* = 9.5 Hz ^{1}H), 4.11 (m, 2H); ^{31}P{^{1}H}NMR (162 MHz, 298 K, deuterium oxide, δ /ppm) 3.37 , 2.96 , 2.18 , -4.96 , -8.36 (d, *J* = 18.2 Hz); HRMS (ESI) calcd for $C_6H_{17}O_{27}P_7$ (M^{2-}) 368.9066, found 368.9065.

InsP stimulated polyP synthesis by isolated vacuoles

For vacuole isolation, the cells were grown in 1 L YPD media at 30 °C overnight, harvested at OD_{600nm} of 0.8-1.9 and vacuoles were isolated as described (*43*). Vacuole concentrations were determined by Bradford assay using BSA as a standard, and reported as concentration of total vacuolar proteins. PolyP synthesis by isolated vacuoles was assessed as described. (*43*). To follow the reaction time-course, 0.04 mg/ml vacuoles were incubated in reaction buffer (10 mM Pipes/KOH pH 6.8, 150 mM KCl, 0.5 mM $MnCl_2$, 200 mM sorbitol) containing an ATP-regenerating system (1 mM ATP-$MgCl_2$, 40

mM creatine phosphate and 0.25 mg/ml creatine kinase) at 27 °C and in the presence or absence of 0.5 μM 5-$InsP_7$. At the indicated time points, 80 μl aliquots were mixed with 160 μl of stop solution (10 mM Pipes/KOH pH 6.8, 150 mM KCl, 200 mM sorbitol, 12 mM EDTA, 0.15 % (v/v) Triton X-100 and 15 μM DAPI) in a black 96-well plate. Samples were allowed to equilibrate for 15 min in the dark and fluorescence of the polyP-DAPI complex was measured in a SPECTRAmax GEMINI XS fluorescence plate reader (Molecular Devices) using λ_{ex} = 415 nm, λ_{em} = 550 nm (cutoff = 530 nm) at 27 °C. The amount of synthesized polyP was calculated from a calibration curve prepared with synthetic polyP-60 (Regenetiss Inc.). PolyP synthesis activity is expressed as nmol polyP per μg of vacuolar protein. To examine the effects of ligand concentrations, the aforementioned reaction mixtures were prepared with serial dilutions of the indicated ligands. In these experiments the ionic strength of the solution was kept at 300 mM by adjusting the KCl concentration accordingly. The reactions were started by adding vacuoles to a final concentration of 0.02 mg/ml (Fig. 2A) or 0.005 mg/ml (Fig. S7). After 10 min of incubation at 27 °C, reactions were stopped and polyP was measured. To prepare stock solutions, 100 mM PP_i or PPP_i were mixed with 100 mM Pipes and the pH was adjusted to 6.8 with NaOH. PP_i and PPP_i were purchased from Sigma, $InsP_6$ was from Calbiochem, 1,4,5-$InsP_3$, 1,4,5,6-$InsP_4$ and 1,3,4,5,6-$InsP_5$ were from SiChem.

Isothermal Titration Calorimetry (ITC)

ITC experiments were performed using a Nano ITC calorimeter (TA Instruments). Proteins were dialyzed against ITC buffer (20 mM Hepes/NaOH 7.0, 200 mM NaCl, 0.25 mM TCEP) prior to all titrations. Experiments were done at 25 °C. 10 μL of $InsP_6$ at 270 μM and 2 mM was injected into 40 μM wild-type or mutant SPX^{ScVtc2}, respectively. The $InsP_5$, $InsP_4$, $InsP_3$, $NaPPP_i$, $NaPP_i$ binding was tested using a ligand concentration of 2mM in the syringe and 200 μM wild-type SPX^{ScVtc2} in the cell. In the case of SPX^{CtVtc4}, protein concentrations were reduced to 10 μM vs. 100 μM $InsP_6$. For SPX^{CtGde1} titrations, 60 μM of protein solution was dialyzed against ITC buffer containing 300mM NaCl and titrated using a 400 μM $InsP_6$ stock. OsPHR2 at a concentration of 50 μM and OsSPX4 (75 μM) were added to the instruments cell. 10 μL of InsP ligands (500 μM), ATP (2 mM), $NaPPP_i$ (2 mM), $NaPP_i$ (5 mM) or NaP_i (5 mM) were injected in time intervals of

150 s. After subtracting heat enthalpies for titrations of ligand into buffer, the ITC data were analyzed using the NanoAnalyze Data Analysis software provided by the manufacturer. The binding affinity of OsSPX4 for OsPHR2, was estimated by injecting OsSPX4 (500 μM) into a OsPHR2 solution in the cell (50 μM) and in the presence and absence of 100 μM 5-$InsP_7$. $InsP_6$, $NaPPP_i$, $NaPP_i$ were purchased from Sigma, $InsP_5$, $InsP_4$, $InsP_3$ were purchased from SiChem.

Microscale thermophoresis (MST)

Binding of $InsP_6$ and 5-$InsP_7$ by SPX^{ScVtc2} was measured by microscale thermophoresis. 50 nM of protein was preincubated with 50 nM trisNTA-Oregon Green488 (*44*) for 15 min. on ice in a buffer containing 25 mM Hepes/NaOH pH 7.0, 250 mM NaCl, 0.1 mg/ml BSA, 0.05% Tween-20. Then the mixture was centrifuged for 10 min. at 22,000 xg in order to remove protein aggregates and mixed with the serial dilutions of ligand in water. The reaction mixture was loaded into Monolith NT Premium Coated Capillaries (NanoTemper Technologies GmbH) and Thermophoresis was measured using a Monolith NT.115 instrument (NanoTemper Technologies GmbH) at an ambient temperature with 5s/30s/5s laser off/on/off times, respectively. The LED power was set to 50%, MST laser power was set to 30% and Thermophoresis + T-Jump signal from 3 independent experiments was fitted into a full single-site binding equation using GraphPad Prism 5 software. No ligand-dependent changes of fluorescence signal were observed.

To measure $InsP_6$ and 5-$InsP_7$ binding by the OsSPX4-OsPHR2 complex, OsPHR2 was covalently labeled using Monolith™ Protein Labeling Kit RED-MALEIMIDE (NanoTemper Technologies GmbH). 100 nM of the labeled OsPHR2 was mixed with 100 nM of unlabeled OsSPX4 in buffer containing 20 mM Tris/HCl pH 8.0, 150 mM KCl, 0.25 mM TCEP, 0.1 mg/ml BSA and 0.05% Tween20. Then the mixture was centrifuged for 10 min. at 22,000 xg, mixed with serial dilutions of the ligands in water and thermophoresis was measured as described above, except that LED power was set to 20%, and MST laser power was set to 50%. Ligand-dependent changes of fluorescence did not exceed 12%. Background-corrected Thermophoresis + T-Jump signals from 3

independent experiments were fitted into a full single-site binding equation. $InsP_6$ was purchased from Calbiochem.

Generation of Vtc3 and Vtc4 SPX domain mutants in yeast

Yeast mutant strains were constructed based on a BY4742 Δvtc2, Δvtc3, Δvtc4 strain.Yeast strain BY4742 vtc2::LEU2 vtc3::natNT2 vtc4::kanMX was constructed from the BY4742 vtc4::kanMX strain (Euroscarf) by replacing the complete open reading frames of VTC2 and VTC3 genes with a corresponding marker cassette (*45*). Wild-type or mutant VTC3 and VTC4 genes under the control of endogenous promoters were introduced by genomic integration of pRS306 and pRS303 plasmids, respectively. Double mutants containing the corresponding mutations of equivalent residues in Vtc3 and Vtc4 were used for the analysis, targeting two SPX domains of the VTC complex simultaneously. Mutant protein levels on isolated vacuoles were determined by western blotting using Vam7 as a reference and were found to be 40-90% of the levels in the reconstituted wild-type Vtc3/Vtc4 (wt/wt). The activities measured were corrected for these moderate differences in VTC abundance on isolated vacuoles.

Expression and analysis of PHO1 mutants in Arabidopsis

A cassette containing the coding genomic region of PHO1 fused to GFP and a 6xHis-StrepII tag was inserted in a modified pMDC32 binary (*46*) vector containing a 2.1 kbp of the PHO1 promoter. Mutations within the PHO1 SPX domain were introduced using the In-Fusion cloning method. The resulting constructs were transformed into the Arabidopsis *pho1-2* mutant using *Agrobacterium tumefaciens* strain pGV3101 and the floral dip method (*47*). T2 transgenic plants were selected by placing seeds on agar-solidified medium containing 30 μg/ml hygromycin for 7 days followed by transfer of plantlets to soil and growth in a phytotron with a day/night cycle of 10 h / 14 h and a light intensity of 150 $\mu mol \cdot m^{-2} s^{-1}$. P_i concentration in leaves was measured by the molybdate assay (*48*). Localization of PHO1-GFP in roots was assessed by confocal microscopy using a Zeiss LSM 700 confocal microscope (Zeiss, Jena, Germany) with an Apochromat 63× Water immersion DIC objective with a 1.2 NA. Images were processed using NIH

ImageJ software. To analyze PHO1 expression level in roots by Western blot, plants were first selected on agar-solidified hygromycin plates and then shifted to wide-mouth Erlenmeyer flasks containing 15-20 mL half-strength Murashige and Skoog liquid medium and 1 % sucrose to produce large amounts of roots from intact plants. Proteins were extracted from homogenized 25 d old roots at 4 °C in extraction buffer containing 10 mM phosphate buffer pH 7.4, 300 mM sucrose, 150 mM NaCl, 5 mM EDTA, 5 mM EGTA, 1 mM DTT, 20 mM NaF and 1× protease inhibitor (Roche EDTA free complete mini tablet), and sonicated for 10 min in an ice-cold water bath. The lysates were centrifuged for 5 min at 6,000 xg and the resulting supernatant was centrifuged again for 60 min at 21,000 xg to obtain microsomal fractions. Fifty microgram of protein were separated on a SDS-PAGE and transferred to an Amersham Hybond-P PVDF membrane (GE healthcare). The rabbit polyclonal antibody THETM Anti-GFP (Genscript, 1:5,000 dilution) and goat anti-rabbit IgG-HRP (Santa Cruz Biotechnology, USA, 1:7,500 dilution) were used along with the Western Bright Sirius HRP substrate (Advansta, USA). Signal intensity was measured using a GE healthcare ImageQuant RT ECL Imager. For analysis of the expression of the *IPS*, *SPX3* ad *MGD3* genes by q-RT-PCR, 7 d old seedlings grown-on agar-solidified plates were harvested and total RNA was isolated. Quantitative real-time RT-PCR analysis was performed using a Stratagene Mx3005P™ qPCR System (Stratagene, La Jolla, USA) and SYBR select master mix (Applied Biosystems). For the normalization of gene transcripts, *ACTIN2* was used as an internal control. 3-5 independent lines were used for qPCR experiments.

Pull-down experiments

Pull-downs were performed using recombinant full-length OsSPX4 (residues 1-320) carrying a C-terminal HA-fusion tag and coupled to μMACS HA magnetic beads (Miltenyi Biotec). One reaction contained 80 μL anti-HA beads, 2 μg OsSPX4, 4 μg of full-length untagged OsPHR2 (residues 1-426), 20 μM ligand (5-InsP$_7$ or P$_i$), 20 mM Tris/HCl pH 8.0, 150 mM KCl, 0.5 mM TCEP, 0.5% (v/v) IGEPAL in a total volume of 1 mL. Reaction mixtures were incubated for 30 min at 4 °C on a rotating wheel. Beads were onto a magnetic column and the column was washed with 5x 200 μL of washing buffer (20 mM Tris/HCl pH 8.0, 150 mM KCl, 0.5 mM TCEP, 0.5% (v/v) IGEPAL,

supplemented with either 20 μM 5-$InsP_7$ or P_i) and eluted in 70 μL preheated (95 °C) SDS sample buffer. Elutions were analyzed by SDS PAGE, using 2 μg OsSPX4-HA and 4 μg OsSPX4-HA as loading input controls.

Determination of $InsP_7$ levels *in vivo*

Precultures were grown in Synthetic Complete (SC) medium without inositol for 24 h at 30°C and inoculated into the same medium supplemented with 5 μCi/ml *myo*[1,2-^{3}H(N)] inositol (60 Ci/mmol). The cultures were grown for 18-20 h at 30°C to an OD_{600} of 0.4-1.0. Cells were collected by centrifugation (1,800 xg, 3 min, at room temperature), washed twice with phosphate-free SC medium and resuspended in the same medium supplemented with 5 μCi/ml *myo*[1,2-^{3}H(N)] inositol at an OD_{600} of 0.5. A 10 ml aliquot was supplemented with 10 mM KH_2PO_4 and incubated for 2 h at 30°C to produce a sample of non-starved cells. The rest of the culture was incubated for 2 h in the absence of phosphate, and then a 10 ml sample of starved cells was withdrawn The cells were collected, washed twice with the respective growth medium and stored at -80°C until extraction. 10 mM KH_2PO_4 was added to the remaining 10 ml of the culture and the incubation was continued for1 h to analyze the effect of phosphate re-supply. Inositol polyphosphates were extracted with $HClO_4$ and fractionated by anion-exchange HPLC as described (*49*). The ratio of the radioactivity in $InsP_7$ and $InsP_6$ peaks was determined for all samples. The $InsP_6$ and $InsP_7$ peaks were assigned using radioactive standards. ^{3}H-$InsP_6$ was acquired from PerkinElmer NEN (New England Nuclear) and ^{3}H-$InsP_7$ was prepared using mouse IP6K1 as previously described (*50*).

Supplementary Text

Author Contributions

A.M., Y.P. and M.H. designed the study. R.W. expressed, purified and crystallized proteins, refined crystal structures, performed in vitro pull-down and ITC assays, R.G. analyzed VTC polyP synthesis and performed MST assays, R.G. and Ad. Sa. performed *in vivo* InsP measurements, R.W. and V.T. performed and analyzed NMR experiments, An.Sc. generated and analyzed yeast strains, J.J. performed PHO1 plant experiments, I.P. and H.J.J synthesized 5-$InsP_7$, R.W., R.G., J.J, V.T., Y.P., A.M. and M.H. analyzed data, R.W., R.G., A.M. and M.H. wrote the manuscript. All authors commented on the manuscript.

Supplementary References

31. J. Martinez, V. Truffault, M. Hothorn, *J. Biol. Chem.* **290**, 23348–60 (2015).
32. G. Kustatscher, M. Hothorn, C. Pugieux, K. Scheffzek, A. G. Ladurner, *Nat. Struct. Mol. Biol.* **12**, 624–625 (2005).
33. N. Shaw, C. Cheng, Z.-J. Liu, http://dx.doi.org/10.1038/nprot.2007.287 (2007).
34. W. Kabsch, *J. Appl. Crystallogr.* **26**, 795–800 (1993).
35. A. J. McCoy *et al.*, *J. Appl. Crystallogr.* **40**, 658–674 (2007).
36. P. Emsley, K. Cowtan, *Acta Crystallogr. D Biol. Crystallogr.* **60**, 2126–2132 (2004).
37. I. W. Davis *et al.*, *Nucleic Acids Res.* **35**, W375–383 (2007).
38. T. D. Fenn, D. Ringe, G. A. Petsko, *J. Appl. Crystallogr.* **36**, 944–947 (2003).
39. N. A. Baker, D. Sept, S. Joseph, M. J. Holst, J. A. McCammon, *Proc. Natl. Acad. Sci. U. S. A.* **98**, 10037–10041 (2001).
40. M. F. Sanner, A. J. Olson, J. C. Spehner, *Biopolymers*. **38**, 305–320 (1996).
41. T. Diercks, M. Daniels, R. Kaptein, *J. Biomol. NMR*. **33**, 243–259 (2005).
42. I. Pavlovic *et al.*, *Angew. Chem. Int. Ed Engl.* **54**, 9622–9626 (2015).
43. R. Gerasimaitė, S. Sharma, Y. Desfougères, A. Schmidt, A. Mayer, *J. Cell Sci.* **127**, 5093–5104 (2014).
44. S. Lata, M. Gavutis, R. Tampé, J. Piehler, *J. Am. Chem. Soc.* **128**, 2365–2372 (2006).
45. C. Janke *et al.*, *Yeast*. **21**, 947–962 (2004).
46. M. D. Curtis, U. Grossniklaus, *Plant Physiol.* **133**, 462–469 (2003).
47. S. J. Clough, A. F. Bent, *Plant J.* **16**, 735–743 (1998).
48. B. Ames, *Methods Enzym.* **8**, 115–118 (1966).
49. C. Azevedo, A. Saiardi, *Nat. Protoc.* **1**, 2416–2422 (2006).
50. C. Azevedo, A. Burton, M. Bennett, S. M. N. Onnebo, A. Saiardi, *Methods Mol. Biol. Clifton NJ.* **645**, 73–85 (2010).
51. W. Kabsch, C. Sander, *Biopolymers*. **22**, 2577–2637 (1983).
52. R Core Team, *R: A language and environment for statistical computing. R Foundation for Statistical Computing, Vienna, Austria. 2013* (ISBN 3-900051-07-0, 2014).
53. E. A. Steidle *et al.*, *J. Biol. Chem.* (2016), doi:10.1074/jbc.M116.714907.
54. P. R. Evans, G. N. Murshudov, *Acta Crystallogr. D Biol. Crystallogr.* **69**, 1204–1214 (2013).

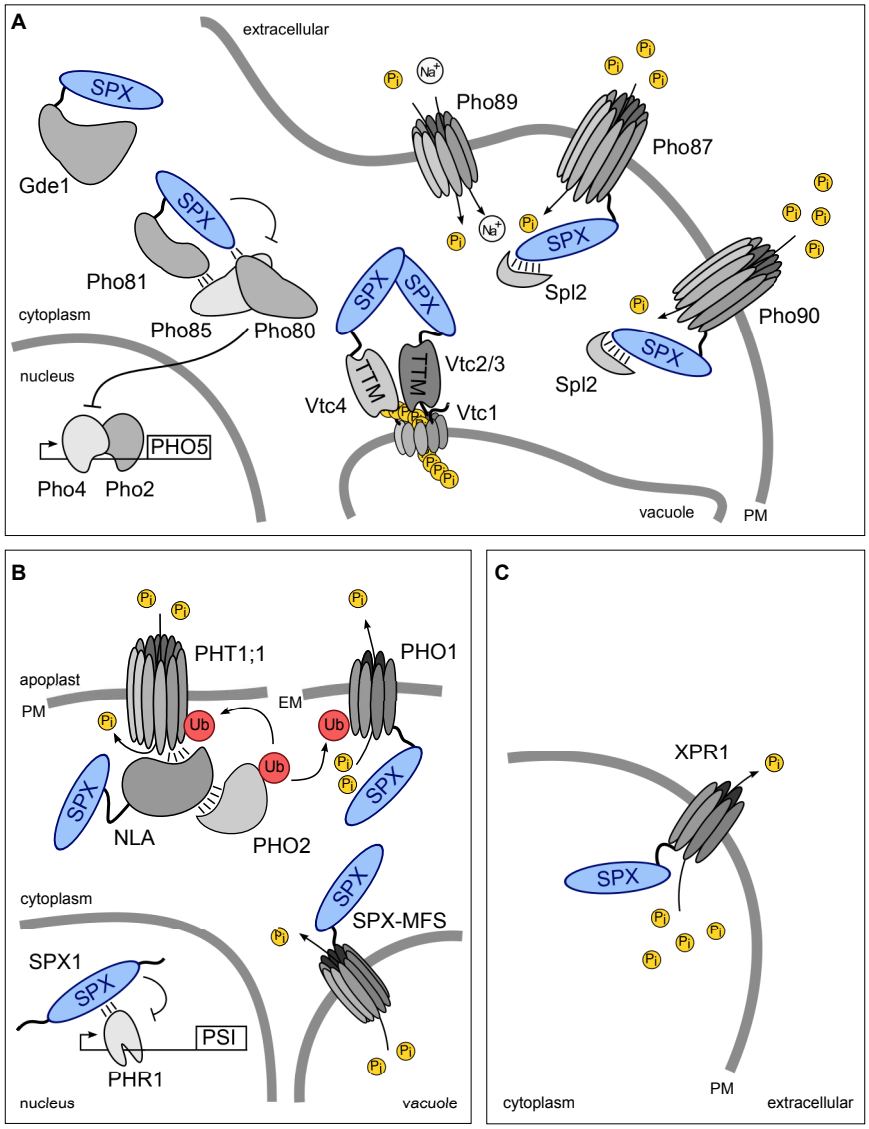

Fig. S1. SPX domain-containing proteins are involved in P_i homeostasis. Schematic overview of SPX-domain containing proteins: The name SPX refers to **S**YG1 and **P**ho81 from yeast, and mammalian **X**PR1, all of which contain an N-terminal SPX domain (http://www.ebi.ac.uk/interpro/entry/IPR004331). (**A**) Yeast: P_i is taken up via high- (**Pho**sphate metabolism 89, Pho89) and low-affinity phosphate transporters (**Pho**sphate metabolism 87, Pho87; **Pho**sphate metabolism 90, Pho90). Their SPX domains interact with the Spl2 protein (**S**uppressor of **P**hospho**L**ipase C 1 deletion). The cyclin-dependent kinase inhibitor Pho81 regulates transcription of phosphate-regulated genes (such as the PHO5 gene) via the cyclin-dependent kinases Pho80/Pho85 and the transcription factors Pho2 and Pho4. The glycerophosphodiesterase Gde1 liberates P_i from glycerophosphocholine. The **V**acuolar **T**ransporter **C**haperone (VTC) complex generates polyP for P_i storage in vacuoles. TTM (**T**riphosphate **T**unnel **M**etalloenzyme). (**B**) Plants harbor SPX domains in P_i transporters such as PHO1 (Arabidopsis PHOSPHATE 1) and SPX-MFS (Major Facility Superfamily, http://www.ebi.ac.uk/interpro/entry/IPR011701), and E3 ubiquitin ligases (NLA, **N**ITROGEN **L**IMITATION **A**DAPTATION), which themselves control **PH**osphate **T**ransporter (PHTs) protein levels. Plants also contain small, stand-alone SPX proteins, which interact with P_i-responsive **PH**OSPHATE STARVATION **R**ESPONSE (PHR) transcription factors. Pho2: E2 conjugase. PSI: **P**hosphate-**s**tarvation **i**nduced genes. (**C**) The only SPX domain-containing protein in mammals is the phosphate exporter **X**enotropic and **P**olytropic retrovirus **R**eceptor 1 (XPR1). PM (plasma membrane), EM (endomembrane).

A

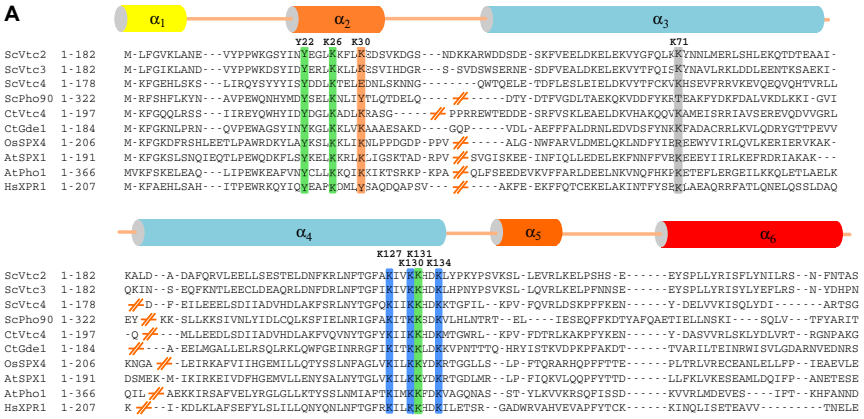

B

protein/ residues/ mutation	tag	organism	Uniprot identifier	express-able
ScPho81 1-199	His [N]	*Saccharomyces cerevisiae*	P17442	-
ScPho81 1-199	Strep [C]	*Saccharomyces cerevisiae*	P17442	-
ScVtc2 1-157	His [C]	*Saccharomyces cerevisiae*	P43585	+/-
ScVtc2 1-177	His [N]	*Saccharomyces cerevisiae*	P43585	-
ScVtc2 1-182	His [C]	*Saccharomyces cerevisiae*	P43585	+
ScVtc2 15-182	His [C]	*Saccharomyces cerevisiae*	P43585	+
ScVtc2 1-182	Strep [C]	*Saccharomyces cerevisiae*	P43585	+/-
ScVtc2 1-553 E475N (catalytic dead)	His [C]	*Saccharomyces cerevisiae*	P43585	+
ScVtc2 1-176	Macro-His [C]	*Saccharomyces cerevisiae*	P43585	-
ScVtc4 1-156	His [C]	*Saccharomyces cerevisiae*	P47075	-
ScVtc4 1-178	His [C]	*Saccharomyces cerevisiae*	P47075	+
ScVtc4 1-178	His-Strep-Thioredoxin [N]	*Saccharomyces cerevisiae*	P47075	+
ScVtc4 1-178	Macro-His [C]	*Saccharomyces cerevisiae*	P47075	+
ScVtc4 1-480 E426N (catalytic dead)	His [C]	*Saccharomyces cerevisiae*	P47075	+
ScVtc4 1-480 E426N (catalytic dead)	Strep [C]	*Saccharomyces cerevisiae*	P47075	-
ScVtc4 1-480 E426N (catalytic dead)	His [N]	*Saccharomyces cerevisiae*	P47075	+
ScVtc4 1-480	His [N]	*Saccharomyces cerevisiae*	P47075	+
ScVtc4 1-480	His [C]	*Saccharomyces cerevisiae*	P47075	+
ScVtc4 189-480	His [N]	*Saccharomyces cerevisiae*	P47075	+
ScPho87 1-383	His [C]	*Saccharomyces cerevisiae*	P25360	+
ScPho90 1-335	His [C]	*Saccharomyces cerevisiae*	P39535	+
CtGde1 1-193	His [C]	*Chaetomium thermophilum*	G0RY29	+
CtVtc4 1-188	His [C]	*Chaetomium thermophilum*	G0SCH1	+
CaSPX1 1-189	His [C]	*Cicer arietinum*	XP_004494019.1*	+/-
CaSPX1 1-189	His [N]	*Cicer arietinum*	XP_004494019.1*	+/-
CaSPX1 1-189	His-Strep-Sumo [N]	*Cicer arietinum*	XP_004494019.1*	+/-
TcSPX 1-188	His [C]	*Theobroma cacao*	gb|EOY25792.1**	-
TcSPX 1-188	His-Strep-Sumo [N]	*Theobroma cacao*	gb|EOY25792.1**	+/-
HsXRP1 1-207	His [C]	*Homo sapiens*	Q9UBH6	+
AtPho1 1-344	His [C]	*Arabidopsis thaliana*	Q8S403	-
AtPho1 1-344	His-Strep-Sumo [N]	*Arabidopsis thaliana*	Q8S403	-
AtPho1 1-364	His-Strep-Sumo [N]	*Arabidopsis thaliana*	Q8S403	-
AtPho1 1-386	His [C]	*Arabidopsis thaliana*	Q8S403	+
AtSPX1 1-159	His [C]	*Arabidopsis thaliana*	Q8LBH4	-
AtSPX1 1-170	His [C]	*Arabidopsis thaliana*	Q8LBH4	-
AtSPX1 1-256	His [C]	*Arabidopsis thaliana*	Q8LBH4	+/-
AtSPX1 1-256	His-Strep-Thioredoxin [N]	*Arabidopsis thaliana*	Q8LBH4	-
AtSPX1 1-256	His-Strep-GB1 [N]	*Arabidopsis thaliana*	Q8LBH4	-
AtSPX1 1-256	Macro-His [C]	*Arabidopsis thaliana*	Q8LBH4	+/-
AtSPX1 1-256	His-Strep-Sumo [N]	*Arabidopsis thaliana*	Q8LBH4	+/-
AtSPX3 1-248	Strep [C]	*Arabidopsis thaliana*	Q5PP62	-
AtSPX3 1-237 codon opt *E.coli*	His [C]	*Arabidopsis thaliana*	Q5PP62	-
AtSPX3 1-179 codon opt *E. coli*	His [C]	*Arabidopsis thaliana*	Q5PP62	-
AtSPX3 1-171 codon opt *E. coli*	Macro-His [C]	*Arabidopsis thaliana*	Q5PP62	-
OsSPX4 1-320	His-Strep-Sumo [N]	*Oryza sativa*	Q10B79	+/-
OsSPX4 1-320	His-Strep-Sumo [N] + HA [C]	*Oryza sativa*	Q10B79	+/-

N: N-terminal
C: C-terminal
Macro: histone macro H2A1.1 domain
GB1: protein G B1 domain

* NCBI identifier
** GenBank identifiers

Fig. S2. A conserved set of lysine residues forms a basic surface ligand binding cluster in SPX domains. (**A**) Sequence alignment of different SPX domains including a secondary structure assignment for SPX^{ScVtc4} calculated with the program DSSP (*51*). Conserved amino acid residues are highlighted in green (phosphate binding cluster, PBC), blue (lysine surface cluster, KSC), orange (semi-conserved surface lysine), gray (structural control mutant, SC). (**B**) Overview of the different SPX domain expression constructs and their biochemical properties.

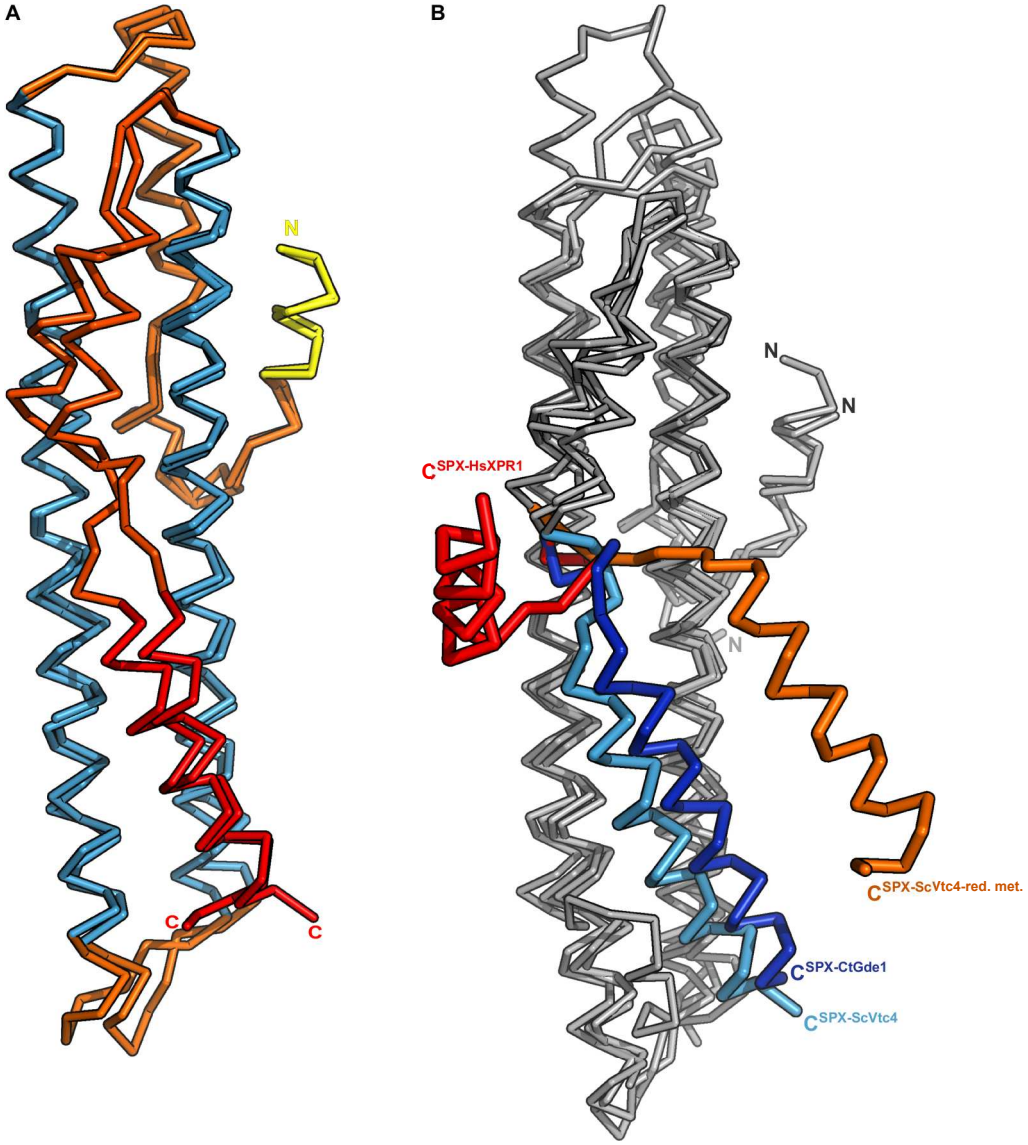

Fig. S3. The C-terminal α6 helix adopts various conformations in different SPX domain structures and crystal forms. (**A**) Structural superposition of crystal forms A and B of SPX^{ScVtc4} crystallized in fusion with the catalytic TTM domain (r.m.s.d. is 1.6 Å comparing 170 corresponding C_α atoms). Shown are C_α traces colored according to Figure 1A. (**B**) Structural superpositions of SPX^{ScVtc4} form A (in light-blue) with ScVtc4 form C obtained by carrier driven crystallization (in orange, r.m.s.d. is 2.2 Å comparing 135 corresponding C_α atoms), with SPX^{CtGde1} (in dark-blue; r.m.s.d. is 2.3 Å comparing 141 corresponding C_α atoms), and SPX^{HsXPR1} (in red; r.m.s.d. is 1.6 Å comparing 147 corresponding C_α atoms), indicates that the C-terminal α6 helix can adopt different orientations.

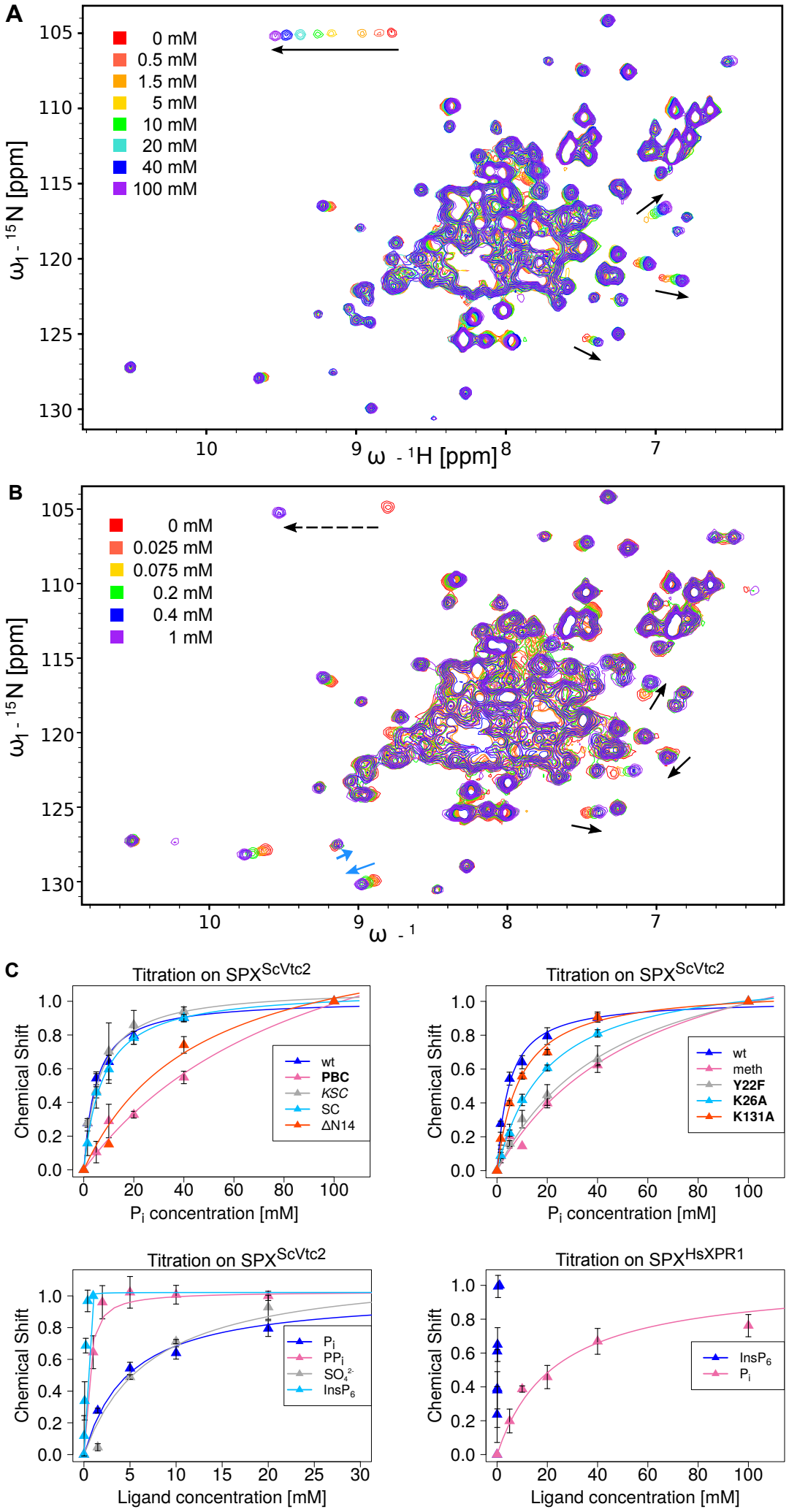
A
0 mM
0.5 mM
1.5 mM
5 mM
10 mM
20 mM
40 mM
100 mM
ω1 - 15N [ppm]
ω - 1H [ppm]
B
0 mM
0.025 mM
0.075 mM
0.2 mM
0.4 mM
1 mM
ω1 - 15N [ppm]
ω - 1
C
Titration on SPXScVtc2
Chemical Shift
Pi concentration [mM]
wt
PBC
KSC
SC
ΔN14
Titration on SPXScVtc2
wt
meth
Y22F
K26A
K131A
Titration on SPXScVtc2
Pi
PPi
SO4 2-
InsP6
Ligand concentration [mM]
Titration on SPXHsXPR1
InsP6
Pi

Fig. S4. Yeast and human SPX domains bind phosphate-containing ligands. Overlay of SPX^{ScVtc2} efb-^{15}N-HSQC NMR spectra recorded in the presence of different (**A**) P_i and (**B**) $InsP_6$ concentrations. Prominent peak-shifts are highlighted by blue ($InsP_6$-specific) and black (common to P_i and $InsP_6$) arrows. (**C**) Normalized chemical shifts were plotted against their corresponding ligand concentrations and fitted using a 1:1 binding model. Data were visualized with the program R (*52*).

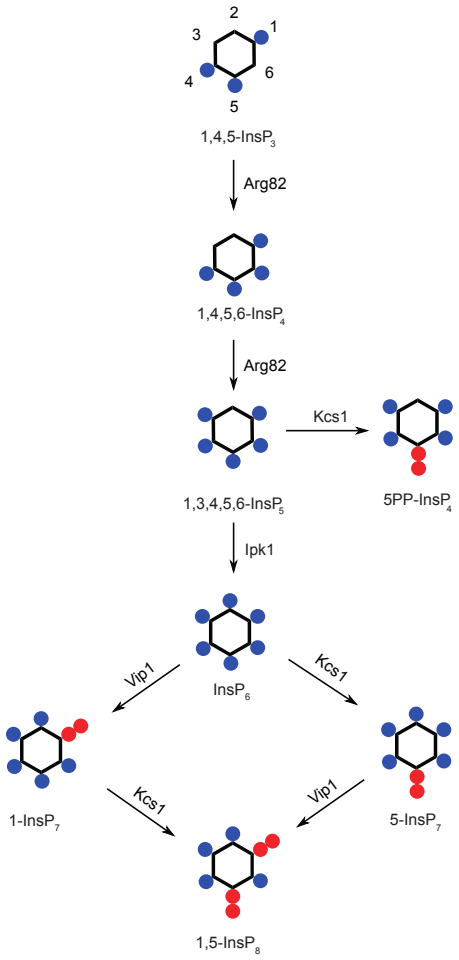

Fig. S5. Schematic representation of known inositol polyphosphate and -pyrophosphate synthesis pathways in yeast. (modified from (*53*).)

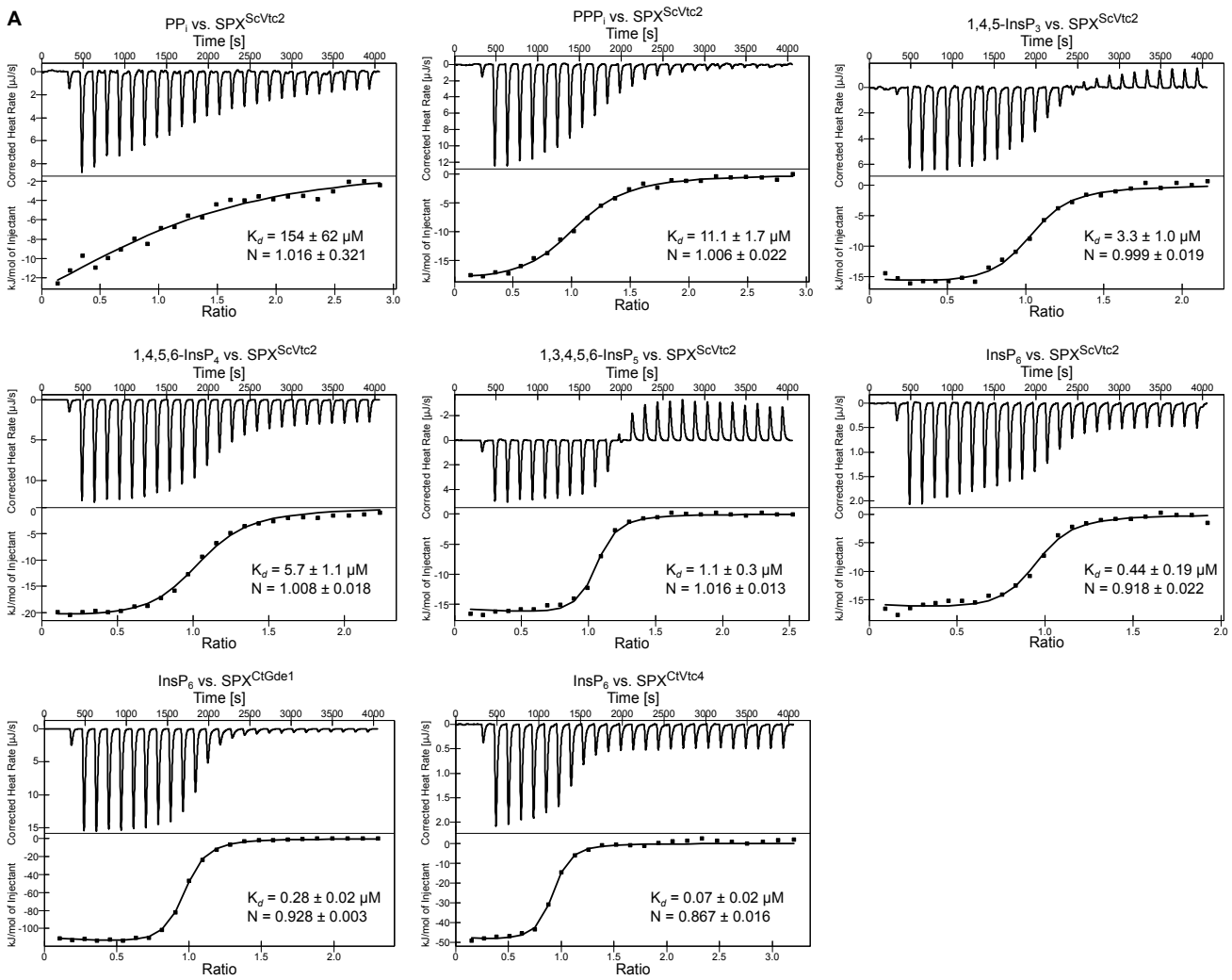
A
PPi vs. SPXScVtc2
Kd = 154 ± 62 µM
N = 1.016 ± 0.321
PPPi vs. SPXScVtc2
Kd = 11.1 ± 1.7 µM
N = 1.006 ± 0.022
1,4,5-InsP3 vs. SPXScVtc2
Kd = 3.3 ± 1.0 µM
N = 0.999 ± 0.019
1,4,5,6-InsP4 vs. SPXScVtc2
Kd = 5.7 ± 1.1 µM
N = 1.008 ± 0.018
1,3,4,5,6-InsP5 vs. SPXScVtc2
Kd = 1.1 ± 0.3 µM
N = 1.016 ± 0.013
InsP6 vs. SPXScVtc2
Kd = 0.44 ± 0.19 µM
N = 0.918 ± 0.022
InsP6 vs. SPXCtGde1
Kd = 0.28 ± 0.02 µM
N = 0.928 ± 0.003
InsP6 vs. SPXCtVtc4
Kd = 0.07 ± 0.02 µM
N = 0.867 ± 0.016
Time [s]
Corrected Heat Rate [µJ/s]
kJ/mol of Injectant
Ratio

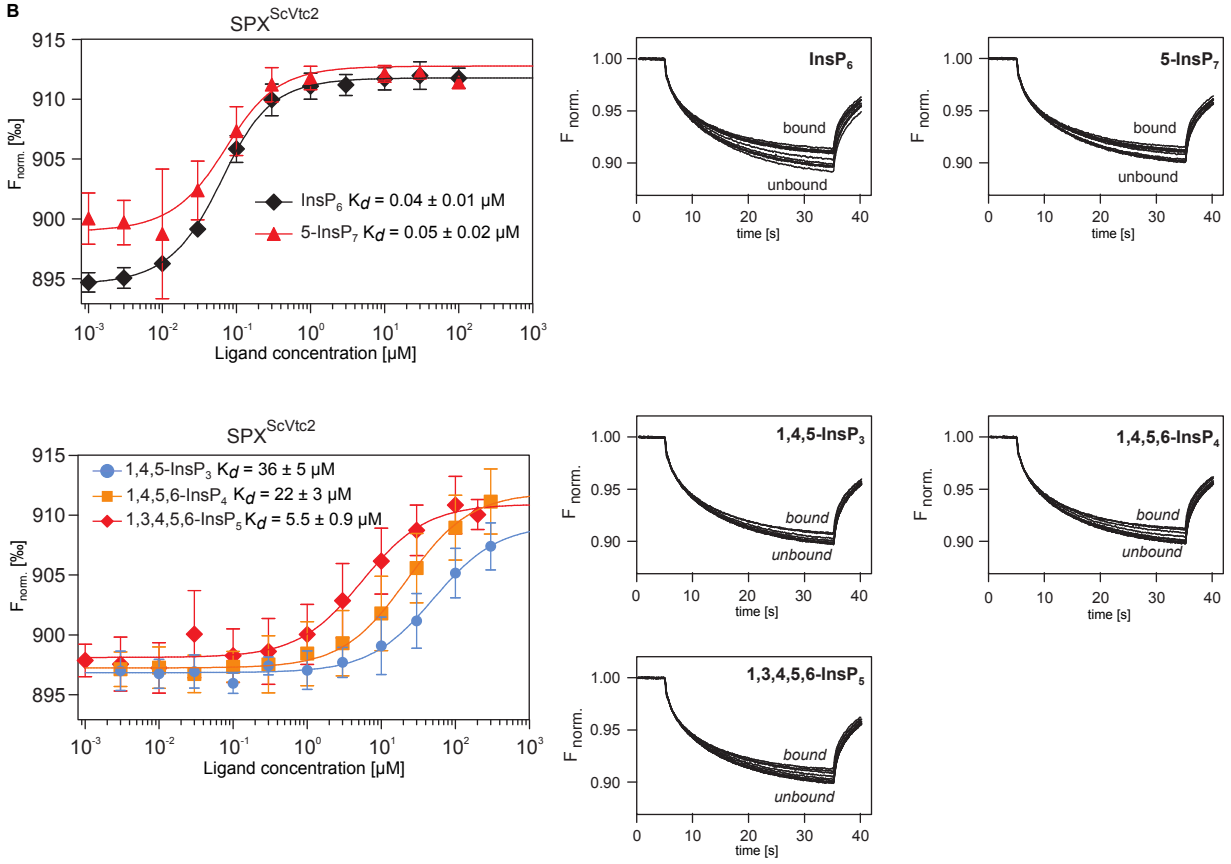
B
SPXScVtc2
InsP6 Kd = 0.04 ± 0.01 µM
5-InsP7 Kd = 0.05 ± 0.02 µM
1,4,5-InsP3 Kd = 36 ± 5 µM
1,4,5,6-InsP4 Kd = 22 ± 3 µM
1,3,4,5,6-InsP5 Kd = 5.5 ± 0.9 µM
Fnorm. [‰]
Ligand concentration [µM]
InsP6
5-InsP7
1,4,5-InsP3
1,4,5,6-InsP4
1,3,4,5,6-InsP5
bound
unbound
Fnorm.
time [s]

Fig. S6. SPX domains bind inositol polyphosphate ligands. (**A**) Isothermal titration calorimetry thermographs (upper panel) and fitted data (lower panel) of different SPX domains vs. different P_i-containing ligands. K_d (dissociation constant), N (stoichiometry) (± fitting errors)(**B**) Analysis of SPX^{ScVtc2} interaction with different InsP ligands by microscale thermophoresis. Shown are raw and fitted data (n=3, ± SD). A complete overview of these experiments can be found in Table S2.

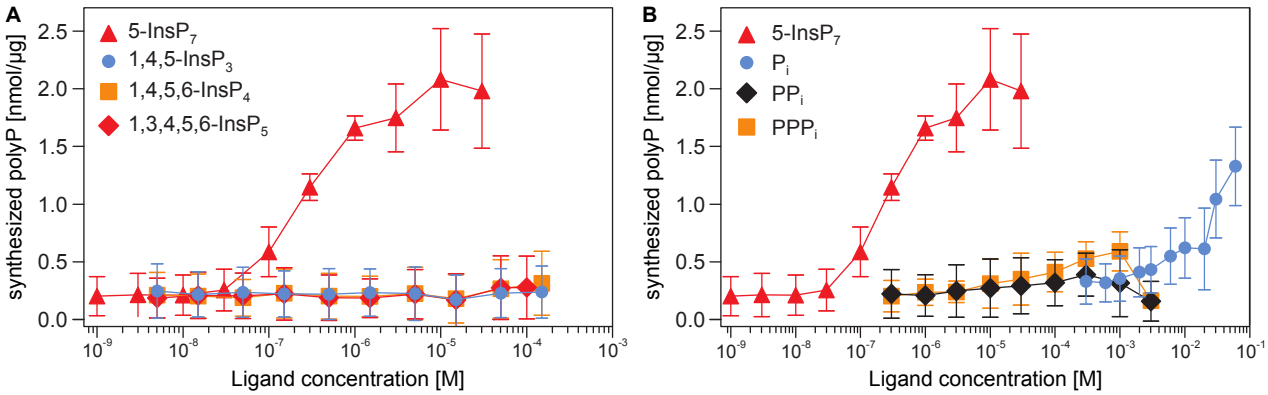

Fig. S7. Stimulation of VTC-catalyzed inorganic polyphosphate synthesis by different phosphate-containing ligands. VTC-dependent polyP synthesis by isolated yeast vacuoles in response to increasing concentrations of (**A**) externally supplied 5-$InsP_7$, $InsP_5$, $InsP_4$ and $InsP_3$ or (**B**) PPP_i (triphosphate), PP_i (pyrophosphate) and P_i. The titration with 5-$InsP_7$ from A is shown again for comparison. (n=3, ± SD).

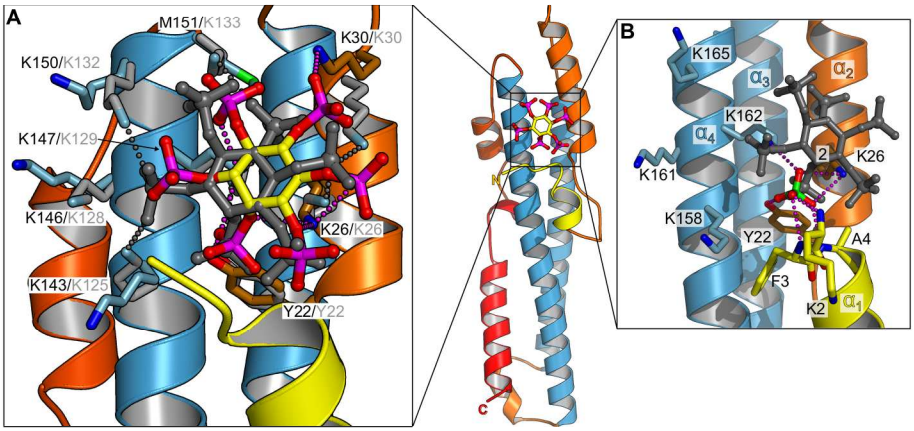

Fig. S8. Comparison of the different $InsP_6$ and sulfate-bound SPX domain structures. An overview of the SPX^{CtGde1} – $InsP_6$ complex (ribbon diagram, colors as in Fig. 1, $InsP_6$ in bonds representation) is shown in the center. (**A**) Detailed view of a structural superposition of SPX^{CtGde1} (in gray) and SPX^{CtVtc4} (colors as in Fig. 1) both bound to $InsP_6$ (in bonds representation) and including interacting side-chains (in bonds representation, black labels SPX^{ScVtc4}, gray labels SPX^{CtGde1}). Hydrogen bonds are highlighted in gray (SPX^{CtGde1}) and magenta (SPX^{CtVtc4}), respectively). R.m.s.d. is 1.9 Å comparing 145 corresponding C_α atoms. (**B**) Structural superposition of SPX^{CtGde1} – $InsP_6$ (in gray) with SPX^{HsXPR1} (ribbon diagram, colors as in A) in complex with a sulfate ion (in green) (r.m.s.d. is 1.5 Å comparing 140 corresponding C_α atoms) reveals the position of the P_i binding cluster (hydrogen bond interactions in magenta). The only axial phosphate group of $InsP_6$ (at the C2 position) is anchored in the PBC pocket occupied by a sulfate ion in our SPX^{HsXPR1} complex structure, formed by the N-terminus of the protein, by Tyr22, Lys26 and by a conserved lysine residue originating from helix α4. This and our NMR experiments together suggest that the InsP axial phosphate is specifically recognized by SPX domains.

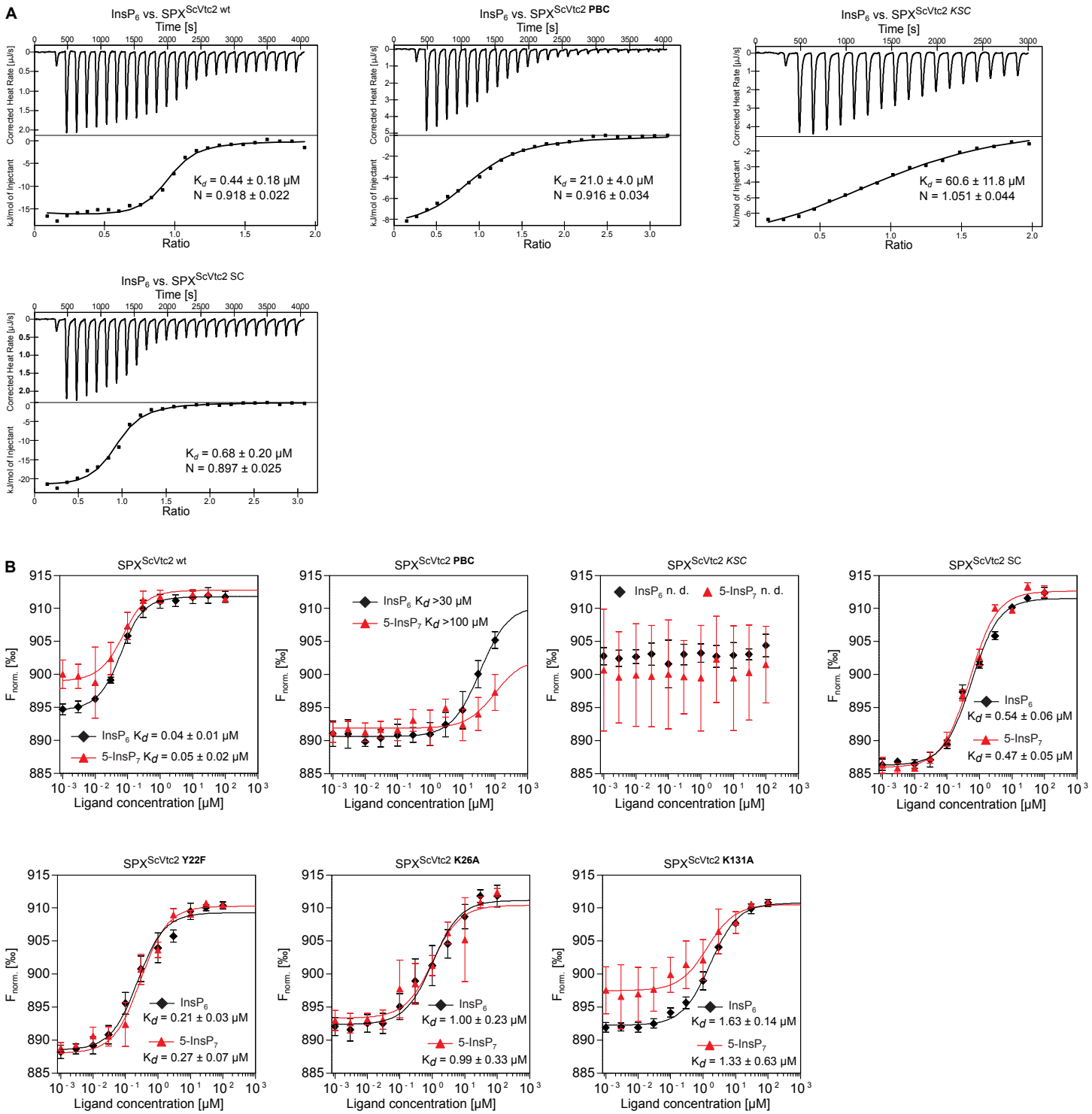

Fig. S9. Substitutions in the SPX basic surface cluster impair $InsP_6$ and 5-$InsP_7$ binding to SPX^{ScVtc2}. (**A**) Isothermal titration calorimetry thermographs (upper panel) and fitted data (lower panel) of wild-type and mutant SPX^{ScVtc2} vs. $InsP_6$. K_d (dissociation constant), N (stoichiometry) (± fitting errors) (**B**) Microscale thermophoresis analysis of wild-type and mutant SPX^{ScVtc2} vs. $InsP_6$ and 5-$InsP_7$. (n=3, ± SD, n.d. no detectable binding). A complete overview of these experiments can be found in Table S3.

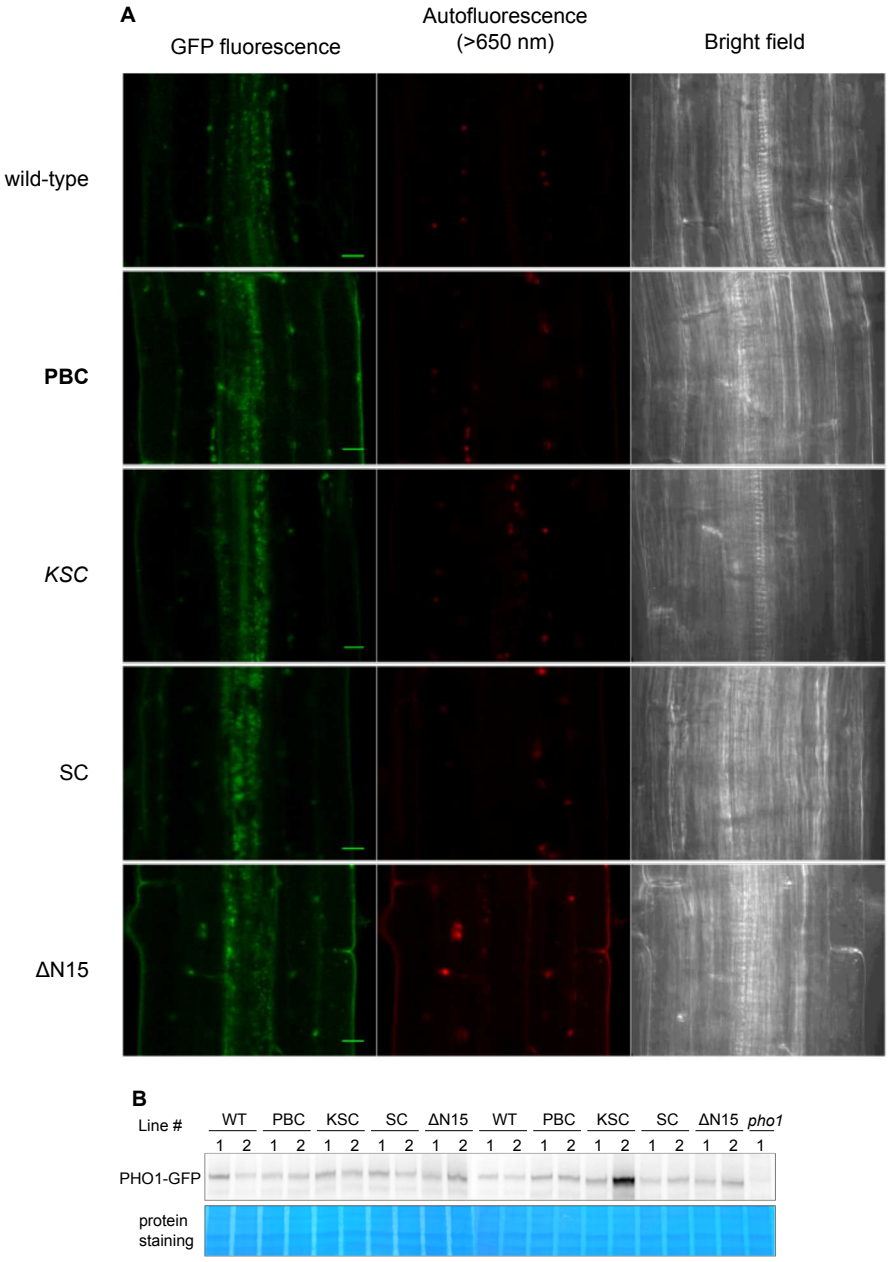

Fig. S10. Point mutations in the putative SPX^{AtPHO1} InsP binding site do not affect localization of full-length AtPHO1 in root pericycle cells. (**A**) AtPHO1 wild-type and mutant proteins were expressed in the *pho1-2* knock-out background with a C-terminal GFP tag under the control of its native promoter. Scale bar = 10 µm. (**B**) Expression level of PHO1-GFP proteins expressed in *pho1-2* transgenic lines, carrying promPHO1::PHO1:GFP (either wild-type or mutated), detected by a polyclonal anti-GFP antibody.

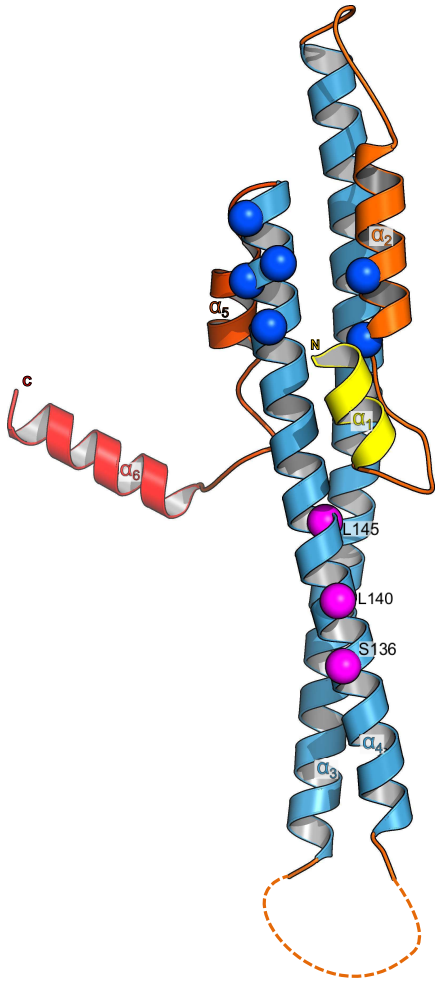

Fig. S11. Structural mapping of human XPR1 patient mutations. Shown is a ribbon diagram of SPX^{HsXPR1} colored as in Fig. 1. Blue spheres indicate the positions of residues involved in InsP binding, magenta spheres denote the positions of XPR1 patient mutations (*24*). The location of these mutations suggest that additional interaction surfaces, possibly for XPR1 protein interaction partners, could be located along the central α4 helix.

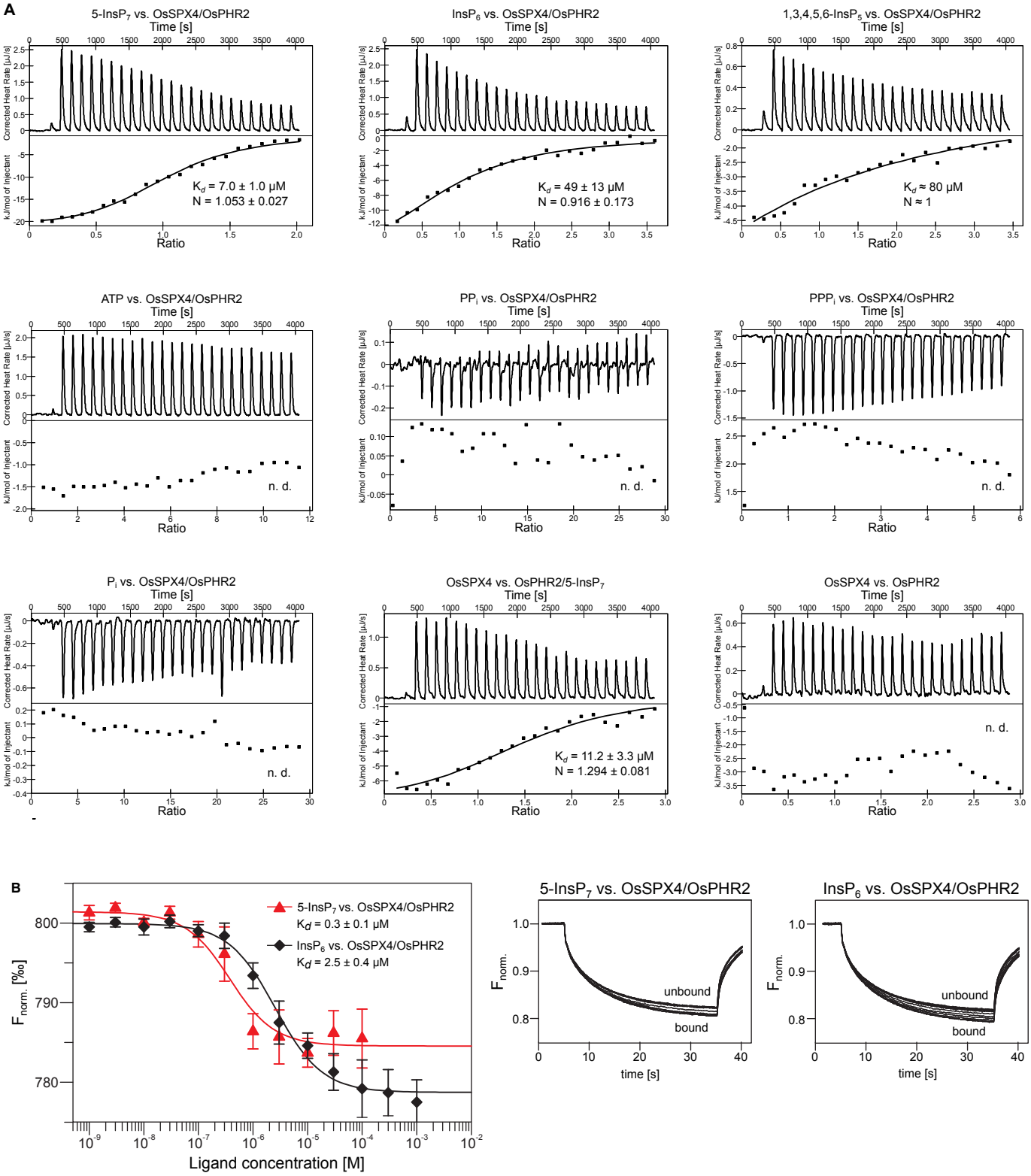

Fig. S12. The OsSPX4 – OsPHR2 complex senses inositol pyrophosphate ligands. (A) Isothermal titration calorimetry thermographs (upper panel) and fitted data (lower panel) of OsSPX4 and OsPHR2 vs. different P_i-containing ligands. K_d (dissociation constant), N (stoichiometry) (± fitting errors, n.d. no detectable binding) (B) Microscale thermophoresis of OsSPX4 and OsPHR2 vs. different InsP ligands. Shown are raw and fitted data, 5-$InsP_7$ and $InsP_6$ measurements were performed with n=3. (error bars ± SD). A table summary of these experiments can be found in Fig. 4B.

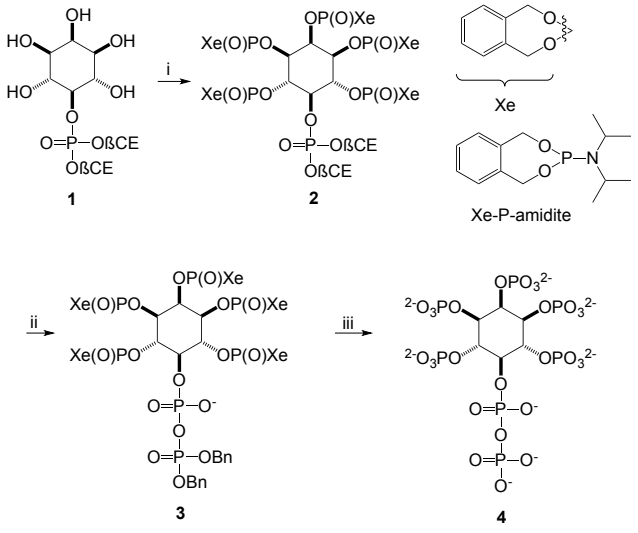

Fig. S13. Chemical synthesis of 5-InsP$_7$. Novel synthetic approach for the preparation of highly pure 5-InsP$_7$: i) Xe-P-amidite, DCI, then *m*CPBA, 93% yield; ii) DBU, BSTFA, then MeOH, TFA, then Bn$_2$-P-Amidite, tetrazole, then *m*CPBA, 58% yield; iii) $NaHCO_3$, H_2O/*t*BuOH Pd(black)/H_2, 64-88% yield.

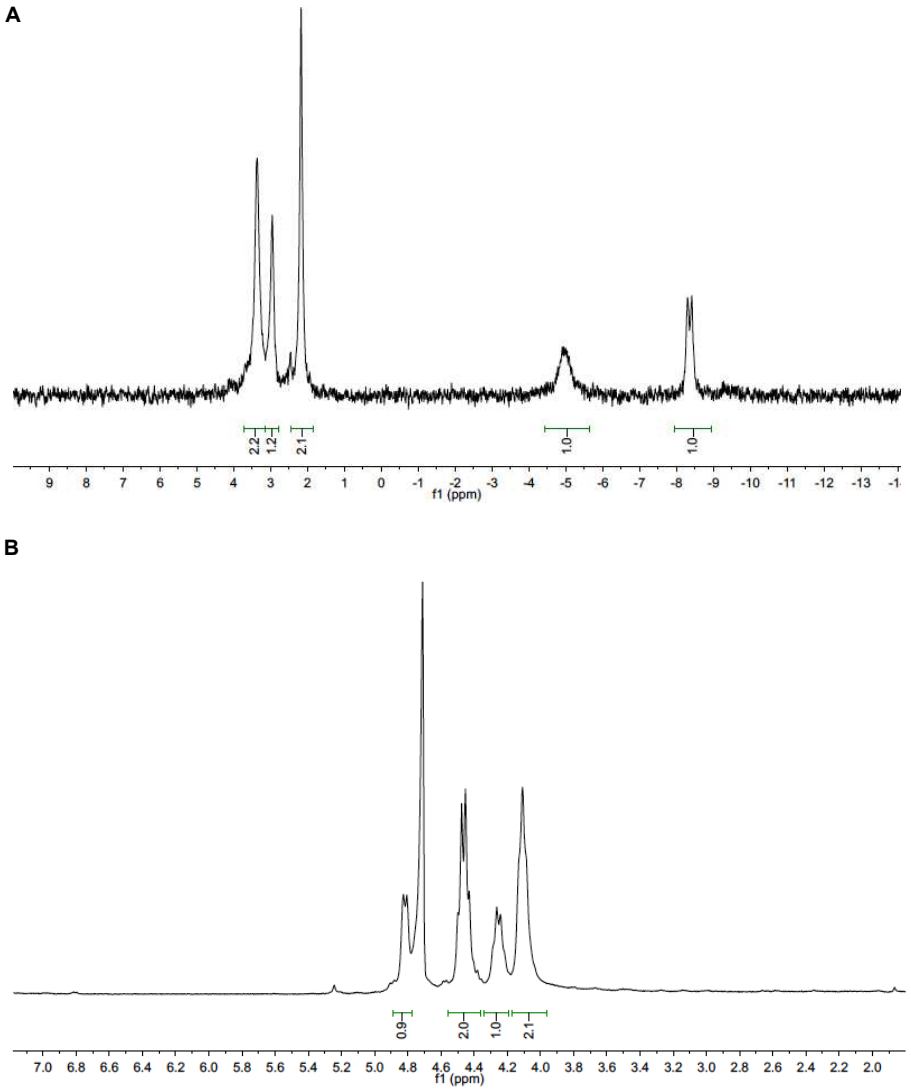

Fig. S14. Analytical data for 5-InsP$_7$. (A) ^{31}P NMR (proton decoupled) of 5-InsP$_7$ in D_2O. (B) ^{1}H NMR (water suppression) of 5-InsP$_7$ in D_2O.

Table S1.

Crystallographic data collection and refinement for 'apo' and ligand-bound SPX domains.

	SPX-TTM^{ScVtc4} (form A)	**SPX-TTM^{ScVtc4} (form B)**	**SPX^{ScVtc4}-macro (red. methylated)**	**SPX^{HsXPR1} SO_4^{2-}**	**SPX^{CtGde1} $InsP_6$**	**SPX^{CtVtc4} $InsP_6$**
Data collection						
Beam-line	PXII	PXIII	ID29	ID29	PXIII	PXIII
Wavelength (Å)	0.999990	1.000020	0.976251	0.976250	1.000000	1.000000
Space-group	$P\,4_3\,2\,2$	$P\,6_4\,2\,2$	$P\,2_1$	$P\,2_1\,2_1\,2_1$	$C\,2$	$P\,6_2$
Resolution (Å)	48.22 – 2.99 (3.17 – 2.99)	19.88 – 3.03 (3.21 – 3.03)	46.86 – 2.13 (2.26 – 2.13)	25.28 – 2.43 (2.49 – 2.43)	19.59 – 1.95 (2.07 – 1.95)	48.63 – 2.75 (2.82 – 2.75)
Unit cell dimensions, a, b, c (Å)	145.39, 145.39, 71.89	92.04, 92.04, 301.73	105.64, 67.92, 129.68	65.950, 80.32, 97.86	89.36, 53.37, 94.31	74.20, 74.20, 74.42
Unit cell dimensions, α,β,γ (°)	90, 90, 90	90, 90, 120	90, 93.32, 90	90, 90, 90	90, 113.42, 90	90, 90, 120
Molecules per AU	1	1	4	2	2 (one bound to $InsP_6$, one 'apo')	1
No. reflections: total	197,009 (30,650)	320,174 (42,687)	688,776 (103,122)	153,559 (10,639)	194,197 (25,612)	503,828 (38,181)
No. reflections: unique	16,084 (2,522)	15,492 (2,337)	101,489 (15,910)	20,166 (1,456)	28,959 (3,947)	6,115 (444)
Completeness (%)	99.8 (99.2)	99.0 (97.4)	99.1 (96.7)	99.8 (99.6)	97.0 (82.8)	99.8 (99.3)
Multiplicity	12.2 (12.2)	20.7 (18.3)	6.8 (6.5)	7.6 (7.3)	6.7 (6.5)	82.4 (13.7)
$I/\sigma I$*	20.2 (1.9)	28.4 (3.0)	15.5 (1.9)	16.7 (1.8)	20.5 (2.3)	43.0 (2.6)
CC(1/2)* (%)	100.0 (74.2)	100 (79.2)	99.0 (80.9)	100.0 (88.4)	100.0 (79.6)	100.0 (91.9)
R_{meas}* (%)	8.6 (133.0)	11.1 (111.0)	8.4 (111.6)	7.2 (120.7)	6.5 (89.4)	14.6 (401.7)
R_{pim}# (%)	3.4 (55.2)	3.3 (33.3)	4.6 (73.9)	3.6 (58.1)	3.5 (59.5)	2.2 (53.1)
Wilson B-factor (Å^2)	96.6	73.5	51.0	65.1	40.8	80.7
Refinement						
No. atoms / No. atoms test set	16,083 / 797	15,497 / 774	101,454/5,074	20,143 / 1,007	27,510 / 1,448	6,111 / 296
Resolution (Å)	48.22 – 2.99	19.88 – 3.03	46.86 – 2.13	25.28 – 2.43	19.59 – 1.95	48.63 – 2.75
R_{cryst} / R_{free}+ (%)	24.4 / 27.3	22.5 / 26.2	21.1 / 24.7	21.75 (23.78)	20.50 (25.09)	22.44 (24.86)
R.m.s. deviations: bond distances+ (Å)	0.024	0.008	0.004	0.010	0.019	0.007
R.m.s. deviations: bond angles+ (°)	0.79	1.00	0.75	1.04	1.40	0.84
Structure/Stereochemistry						
No. atoms: protein	3,851	3,793	11,352	3,039	2,702	1,428
No. atoms: SO_4^{2-}/ $InsP_6$	20	24		10	36	36
No atoms: water			183	43	84	4
Average B-factors: protein (Å^2)	113.7	93.1	58.4	92.0	45.4	87.6
Average B-factors: SO_4^{2-}/$InsP_6$ (Å^2)	149.5	136.0		89.9	78.2	211.1
Average B-factors: water (Å^2)			52.21	79.40	46.19	69.70
Ramachandran plot: most favored regions$ (%)	96.98	96.96	98.95	99.16	98.80	97.11
Ramachandran plot. outliers$ (%)	0.22	0	0	0.56	0	0.58
MolProbity score$	0.89	1.35	1.00	1.04	0.92	1.30
Protein Data Bank ID	**5IIG**	**5IIQ**	**5IIT**	**5IJH**	**5IJJ**	**5IJP**

*as defined in XDS (*34*)
#as defined in Aimless (*54*)
+as defined in autoBUSTER (Global Phasing Limited)
$as defined in Molprobity (*37*)

Table S2.

Binding of P_i-containing ligands to different SPX domains. Comparison of different quantitative binding assays.

Ligand	Nuclear magnetic resonance K_d [µM]	Isothermal titration calorimetry K_d [µM]	Microscale thermophoresis K_d [µM]
P_i	4,800 ± 600; 22,800 ± 300*		
SO_4^{2-}	7,100 ± 300		
PP_i	530 ± 130	154 ± 62	
PPP_i		11.1 ± 1.7	
1,4,5-$InsP_3$		3.3 ± 1.0	36 ± 5
1,4,5,6-$InsP_4$		5.7 ± 1.1	22 ± 3
1,3,4,5,6-$InsP_5$		1.1 ± 0.3	5.5 ± 0.9
$InsP_6$	< 100; < 200*	0.44 ± 0.19; 0.28 ± 0.02**; 0.07 ± 0.02***	0.04 ± 0.01
5-$InsP_7$			0.05 ± 0.02

*SPX^{HsXPR1}
**SPX^{CtGde1}
***SPX^{CtVtc4}

Table S3.

Binding of $InsP_6$ and 5-$InsP_7$ to different mutant SPX^{ScVtc2} proteins. Comparison of three quantitative binding assays.

SPX^{ScVtc2}	**Nuclear magnetic resonance**	**Isothermal titration calorimetry**	**Microscale thermophoresis**	**Microscale thermophoresis**
	K_d [μM] $InsP_6$	K_d [μM] $InsP_6$	K_d [μM] $InsP_6$	K_d [μM] 5-$InsP_7$
wild-type	< 100	0.44 ± 0.18	0.04 ± 0.01	0.05 ± 0.02
PBC (Y22F/K26A/K131)	< 250	21.0 ± 4.0	>30	>100
KSC (K127A/K130A/K134A)	< 250	60.6 ± 11.8	no binding	no binding
SC (K71A)		0.68 ± 0.20	0.54 ± 0.06	0.47 ± 0.05
Y22F			0.21 ± 0.03	0.27 ± 0.07
K26A			1.00 ± 0.23	0.99 ± 0.33
K131A			1.63 ± 0.14	1.33 ± 0.63

Table S4.

Changes of yeast cellular $InsP_7/InsP_6$ levels in response to P_i availability (%).

Strain	non-starved	starved [2 h]	phosphate re-addition [1 h]
BY4741	4.1	1.6	3.7
W303	5.7	1.9	4.3
BY4741 *ipk1Δ*[*]	60	11	43

[*]PP-$InsP_4/InsP_5$